CRANFIELD UNIVERSITY

ELEFTHERIOS GIAKOUMAKIS

TECHNO-ECONOMIC AND ENVIRONMENTAL RISK ASSESSMENT OF A TURBO-ELECTRIC DISTRIBUTED PROPULSION SYSTEM ON A BLENDED WING BODY AIRCRAFT

SCHOOL OF AEROSPACE, TRANSPORT AND MANUFACTURING

MSc by Research
Academic Year: 2013 - 2014

Supervisor: Professor R. Singh, Dr. Nalianda

ABSTRACT

Constant rise of air traffic has caused the environmental impacts of aviation to be the subject of an unprecedented scrutiny. Organisations all over the world are setting targets for emission reductions that represent the technological potential for the next decades. Meeting the stringent goals imposed requires a fundamental shift in approach to engine and aircraft design.

The topic of this research involves the use of the Techno-economic Environmental Risk Analysis (TERA) approach in order to assess the Turbo-electric Distributed Propulsion (TeDP) system. The research will be based on the NASA N3-X concept in terms of dimensions, layout, weighs and performance.

The contribution to knowledge is the development of assessment models to better understand the propulsion and electrical system of the TeDP vehicle. By identifying the key risks and opportunities provided by the technology assessed, this study further contributes to define a technology roadmap for future research.

This research is part of a NASA funding (Grant number: NNX13AI78G) awarded to Cranfield University in order to study Turboelectric Distributed Propulsion using the concept of TERA.

Keywords:

Turboelectric Distributed Propulsion, N3-X, Blended-Wing-Body, Boundary Layer Ingestion, Superconductivity, Liquid Hydrogen, Thrust-Split

ACKNOWLEDGEMENTS

I would like to thank Professor R.Singh for giving me the amazing opportunity to work in such an important project and for all his wise guidance. Working with Professor R.Singh has been a tremendous experience and I can only be thankful for that.

I would like to express my gratitude to supervisor Dr.Nalianda for always being there when I needed help and for the numerous advices at a technical, professional and also personal level.

I would also like to thank Dr.Laskaridis for his precious advices.

Last but not least, I would like to thank my parents for supporting me in all good and difficult moments.

TABLE OF CONTENTS

LIST OF ABBREVIATIONS

ADP	Aerodynamic Design Point
BLI	Boundary Layer Ingestion
BWB	Blended Wing Body
DP	Distributed Propulsion
ETRW	Energy To Revenue Work ratio
FLOPS	Flight Optimization System
FPR	Fan Pressure Ratio
HPC	High Pressure Compressor
HPT	High Pressure Turbine
HTS	High Temperature Superconductivity
BWB	Hybrid Wing Body
IRR	Internal Rate of Return
ISA	International Standard Atmosphere
LCV	Lower Calorific Value
LH_2	Liquid Hydrogen
LHV	Lower Heating Value
LPC	Low Pressure Compressor
LPT	Low Pressure Turbine
LTO	Landing-Takeoff
NPV	Net Present Value
PT	Power Turbine
RTO	Rolling Take-off

SFW	Subsonic Fixed Wing
TeDP	Turboelectric Distributed Propulsion
TERA	Techno-economic, Environmental Risk Assessments
TS	Thrust-Split
TSFC	Thrust Specific Fuel Consumption
TRL	Technology Readiness Level
UHB	Ultra-High Bypass ratio

LIST OF FIGURES

LIST OF TABLES

1 INTRODUCTION

1.1 Background

Since the beginning of commercial aviation in 1920, air traffic has been constantly increasing and numerous forecast studies indicate a similar trend for the next twenty years[5; 58]. The predicted growth in passenger aircraft fleet will push the aeronautics technology to advance more rapidly from economic and environmental viewpoints while ensuring reliable and safe flights.

To address this more stringent environment, NASA Subsonic Fixed Wing (SFW) project has defined four aggressive goals aiming at reducing fuel consumption, emissions, noise and the field length. Table 1 enumerates the performance goals where N+1, N+2, and N+3 represent achieving a "Technology Readiness Level"[44] of 4 to 6 by years 2015, 2020, and 2025 respectively[32]. Traditional tube and wing configurations will accommodate the shortly set N+1 goals, whilst the Hybrid-Wing-Body (BWB) aircraft has been proposed as a more appropriate design to achieve the N+2[33] and N+3[25] goals.

CORNERS OF THE TRADE SPACE	N+1 (2015 EIS) Generation Conventional Tube and Wing (relative to B737/CFM56)	N+2 (2020 IOC) Generation Unconventional Hybrid Wing Body (relative to B777/GE90)	N+3 (2030-2035 EIS) Advanced Aircraft Concepts (relative to user defined reference)
Noise (cum. below Stage 4)	-32 dB	-42 dB	-71 dB or 55 LDN at average airport boundary
LTO NOx Emissions (below CAEP 6)	-60%	-75%	better than -75%
Performance: Fuel Burn	-33%	-40%	better than -70%
Performance: Field Length	-33%	-50%	exploit community airports

Table 1: NASA subsonic transport system level metrics

Meeting the stringent goals imposed requires a fundamental shift in approach to engine and aircraft design. The engine design focuses mainly in increasing the overall efficiency. Engine thermal efficiency has experienced great strides over

the last decades, but only modest gains can be expected through further increase of TET, OPR and components' efficiency. The other half of the engine total efficiency, the propulsive efficiency, is mainly benefited from reduction in specific thrust or increases in the BPR. Increasing the BPR offers fuel burn benefits but there are practical limits to how much it can be increased before significant penalties arise that erode the benefits. Without any revolutionary concepts, soon we will reach a point where the increase of the engine size will counterbalance the benefits from the reduced fuel consumption.

Research has indicated that Turbo-electric Distributed Propulsion (TeDP) on a Blended-Wing-Body (BWB) can circumvent these penalties, lead to a higher effective bypass ratio (eBPR) and can potentially achieve the aggressive N+3 NASA goals.

Cranfield University has undertaken significant research on the subject of Distributed Propulsion (DP) and BWB airframes in the past [6; 24; 26; 37] . Several aspects of DP that have been looked at include modelling the BLI [42], assessing the distortion of the propulsor fan [43] and using CFD studies to investigate the flow inside an S-duct in order to improve the propulsive efficiency and to reduce the overall fuel consumption.

One key variable introduced is the concept of Thrust-Split (TS) that can be defined as the ratio of the thrust produced by the distributed propulsors over the total thrust produced [37; 59].

1.2 Scope of work

The scope of this research is to provide a technical assessment of a conceptual aircraft employing TeDP on a BWB airframe similar to the N3-X configuration as can be seen in Figure 1. This configuration uses remotely located gas-turbine-driven core engines to generate the power required to drive superconducting electrical motors which in turn power an array of propulsor fans. This thesis aims to further the development of the N3-X mainly by considering the use of 100% Liquid Hydrogen as a fuel and through investigating the effect of the TS variable in defining alternative TeDP configurations and providing fuel burn

benefits. Currently, kerosene is used as the main fuel for the N3-X concept while LH2 is utilized for cooling and then it is injected into the core-engines and represents part of the fuel of the aircraft [13; 15]. Assuming that, in the long run, hydrogen will be produced from renewable energy, a transition to hydrogen has the potential to offer fuel burn benefits. The LH2 aircraft has a lower fuel weight than an equivalent kerosene aircraft, but added volume of the fuel tanks might offset the benefits.

This research will require the modelling and simulation of the TeDP vehicle and the assessment of the design parameters that could provide with the optimal fuel burn benefits. To establish the performance of the N3-X, it will be compared to a conventional aircraft (Boeing 777-200LR) and to an unconventional aircraft (N3-A) that uses UHBPR turbofan engines in a BWB airframe.

Figure 1: The N3-X concept (adapted by NASA)

1.3 Objectives

The main aims of this project are to explore technical aspects of a TeDP vehicle on a BWB airframe. The research undertaken will utilise the Techno-economic Environmental Risk Analysis (TERA) approach that combines multiple mathematical models to simulate and optimise the performance of a single or a set of technologies.

The objectives of the research are listed below:

1. Develop a methodology to simulate the TeDP system
2. Investigate the effects of various parameters on the power required by the distributed propulsors and the weight of the TeDP the configuration.
3. Assessment of the effect of efficiency and pressure losses of the distributed propulsors due to BLI
4. Comparisons of the N3-X configurations with baseline aircrafts in terms of fuel burn benefits
5. Investigate the effect of the Thrust-Split ratio
6. Investigate the use of Liquid Hydrogen and the effect on the total mission energy consumption
7. Assessment of the effect of various losses and performance changes at component or subsystem level to the change in total mission energy consumption.

2 LITERATURE REVIEW

2.1 Blended-Wing-Body

The basic concept behind the BWB was first developed in the 1990's by McDonnell Douglas in response to a NASA proposal for advanced, high performance transport aircraft.

Compared to a Tube and Wing (T&W) aircraft carrying the same payload, the BWB's main features are a great Lift to Drag (L/D) ratio of 22[40], noise shielding capabilities[28; 45] and a larger volume that can accommodate embedded engines. The latter can greatly reduce the fuel consumption by enabling Boundary Layer Ingestion (BLI). Additionally, the BWB airframe facilitates the utilisation of LH_2 as fuel due to the large available volume. A very thorough chronicle of the technical development of the BWB was established by Liebeck[28].

2.2 Distributed Propulsion

The BWB configuration is more suitable for achieving the N+2, N+3 goals as the bulky airframe also facilitates the application of innovative concepts such as Distributed Propulsion (DP).

Distributed propulsion is a concept introduced almost as early as flight began. Sehra[55] broadly classified distributed propulsion into three main categories: distributed engines (including small, mini, and micro engine systems), common-core multi-fans, and distributed exhaust. Gohardani [23]produced an extensive list of conceptual and actual aircrafts using distributed propulsion technology that dated from early 20th century. Figure 2 displays the major milestones of distributed propulsion concepts and an extensive historical evolution can be found in Gohardani[23].

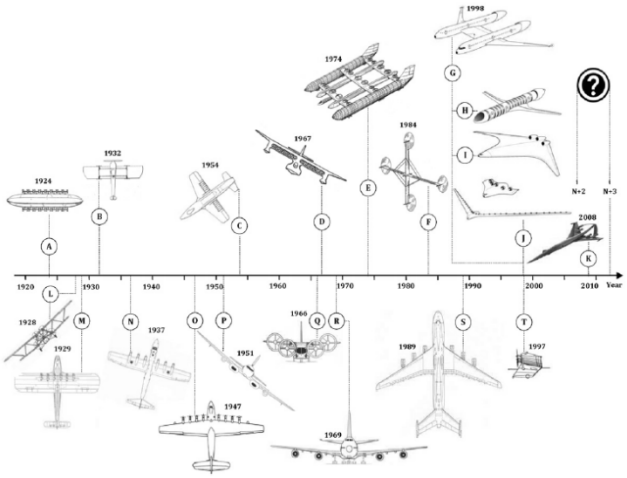

Figure 2: Historical Evolution of Distributed Propulsion Concepts[22]

DP has been suggested as the candidate to successfully address the likelihood of more stringent environmental regulations for commercial aviation. Technical, economical and environmental feasibilities of DP have been ascertained before [7] and it was identified that the main benefit of DP stem from the airframe-propulsion integration. The concept of DP can be described as to “fully integrate a propulsion system within an airframe such that the aircraft takes full synergistic benefits of coupling of airframe aerodynamics and the propulsion thrust stream by distributing thrust using many propulsors on the airframe”[32].

More recently, in 2006, NASA researched and evaluated the synergistic combination of a Distributed Propulsion (DP) configuration on a BWB to yield a Cruise Efficient Short Take-Off and Landing (CESTOL) subsonic transport [31] . This concept adopted a propulsive-airframe-integration (PAI) approach by partially embedding a DP system to achieve benefits in both low-noise short take-off and landing (STOL) operations and efficient high speed cruise [31].

In 2007, Cambridge and MIT launched the Silent Aircraft Initiative (SAI) program to design from scratch an aircraft, having as prior design target to minimise aircraft noise[27]. The selected configuration, named SAX-40, was a BWB with Ultra High By-Pass Ratio (HBPR) embedded engines powering multiple fans with mechanical transmission. The embedded engine system was

preferred mainly to attenuate the rearward turbomachinery noise but it also qualified Boundary Layer Ingestion (BLI). This program assessed for the first time the effects of BLI in ducted turbomachinery.

Next, using the non-proprietary SAX-40 as a starting point, NASA and Boeing studied two BWB configurations; the N2A that used two podded engines in the upper rear fuselage section and the N2B that replaced the podded turbofan engines with embedded engines and boundary layer ingestion offset inlets [36].

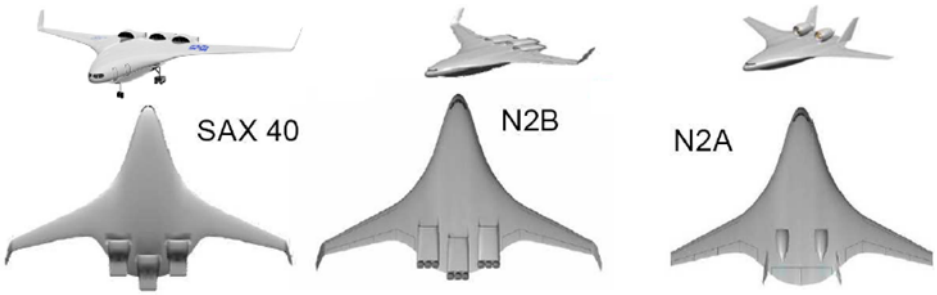

Figure 3: The CMI SAX-40 and Boeing/NASA N2A and N2B BWB Aircraft Concepts [17]

2.3 Turbo-electric Distributed Propulsion

In 2008, NASA proposed a new vehicle in order to improve the vehicle performance enough to meet the N+3 goals. Starting from the airframe of the CESTOL configuration, the new concept introduced two wing-tip mounted engines and a superconducting electrical system to power the distributed fans rather than using a small number of small conventional HBPR engines [34]. Research conducted in 1970 [49] at NASA identified reductions in induced drag of up to 40% if a thrust producing device was located at the wing tip. Other potential benefits include the reduction in both induced drag and tip vortex strength [12] and the nearly elimination of the risk to the rest of the aircraft and passengers in the event of a turbine disk burst. However the wingtip location is not mandatory as there are structural challenges to be overcome.

2.4 The N3-X concept

In a subsequent novel study of embedded superconducting turboelectric propulsion[18], a new concept was formulated by NASA. Based on the N2A airframe, the new concept swapped the pylon mounted turbofan engines and the vertical tails with for a nacelle on the upper aft part of the airframe enclosing the motor-driven propulsors. This reduced the total wetted area of the fans. This merging of the N2A with the superconducting powered CESTOL configuration produced the N3-X aircraft system.

Figure 4: The N3-X concept with Turboelectric Distributed Propulsion [19]

The N3-X is designed to carry 53,000 kg of payload over a distance of 14,000 km at an altitude of 9.4 km and with a Ma number of 0.84.

The motor driven propulsors are embedded in the centre fuselage section near the trailing edge in order to benefit from BLI. The propulsors are housed in a single box nacelle to minimise interference drag between the fan nacelle and the external flows. The number of propulsor fans is not fixed and varies with geometrical and design parameters such as the Fan Pressure Ratio (FPR).

In this concept, NASA [18] uses two Turboshaft engines located at the wingtip in order to “provide wing bending moment relief while the aircraft is in flight and easier access to the turbine engine and superconducting generators”.

2.5 Boundary Layer Ingestion

The idea of applying BLI to aircraft has been known since the early days of jet propulsion[38; 57]. In a BLI configuration, the skin friction drag aft of the distributed propulsors creates boundary layers that slow down the net flow ingested. This reduces the ram drag that enables the engine to produce less gross thrust for the same net thrust. This offers the potential to reduce the power needed to produce the same thrust. The same net thrust can be achieved with lower fuel burn and corresponding reductions in emissions.

Embedding the engines eliminates the pylon or strut which has the potential to reduce the drag and weight. Part of the distributed propulsors is buried in the airframe which reduces even more the drag. An alternative way to present the benefit of BLI comes from re-energizing the aircraft wake, allowing lower energy waste.

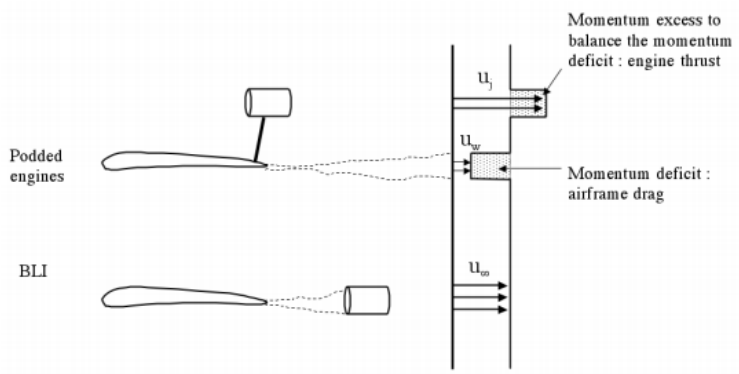

Figure 5: Benefits of BLI-podded case and 100% BLI.

BLI has been modelled with several methods, each of them with their pros and cons. In this research, BLI was taken into account by reducing the inlet Ma number and total pressure seen by the propulsor fans. To illustrate the benefits, a configuration without BLI was introduced in the results.

A consistent treatment of conventionally installed (podded) and highly integrated (embedded engines using BLI) propulsion systems requires a clear definition of the control volumes for correct bookkeeping of thrust and drag. Two

different control volumes have been identified: an inner control volume that encompasses the propulsor only, and an outer control volume that also includes the airframe and the wake[52].

Outer or external control volume

The external control volume includes the airframe, the propulsors and the wake ingested as can be seen in figure 6. The inlet conditions are free-stream and the outlet conditions are assumed at the propulsors exit area (station 4).

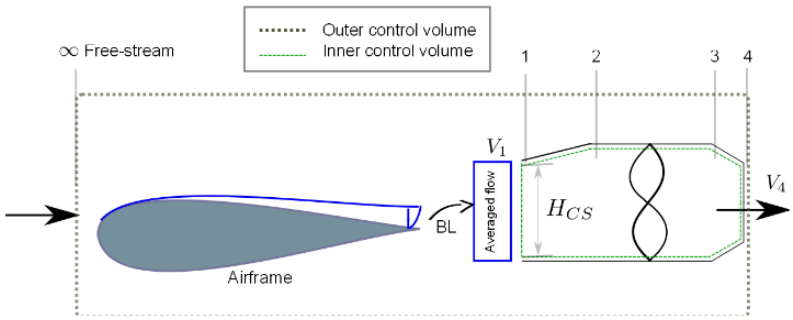

Figure 6: Inner and Outer control volumes for BLI assessment

The external control volume has been studied in [51; 52]. This analysis includes the drag of the wake that is ingested and the difficulty of accounting for the thrust reduction due to BLI with this control volume has motivated the examination of alternative methods based on power balance to examine the benefits of BLI [15].

Inner or internal control volume

In the inner control volume (figure 6), the inlet conditions are set at the station where BL properties are defined (station 1) and the exit conditions are set at the exit of the propulsors (station 4). The main problem of this method is that the conditions at the entrance are unknown.

2.6 Superconductivity

The main enabler of the TeDP system is the use of superconducting motors, generators and transmission lines. Superconductivity is the phenomenon where a material loses all its electrical resistance below a critical temperature and its application has the potential to offer significant gains in power density compared to conventional equipment.

Superconductivity was not overly developed until recently, when it was first demonstrated for marine propulsion [8]. These advancements allowed the consideration of incorporating superconductivity into aircrafts. To achieve this, novel techniques and processes will have to be developed and additional experimental and validation data will be required.

The electrical transmission of power, intrinsically compatible with the emerging concept of DP, allowed the turbine shaft speed to be optimised separately of the fan speed and to be optimised without the usual constraints placed on fan shaft speeds by the fan tip speed limits. The electrical transmission requires a number of superconducting equipment that can be seen in Figure 7. These components include superconducting motors, generators and transmission lines, a cooling system and the distributed fans. Different from conventional transmission system, the power is transferred electrically rather than mechanically through the components that can be seen in figure.

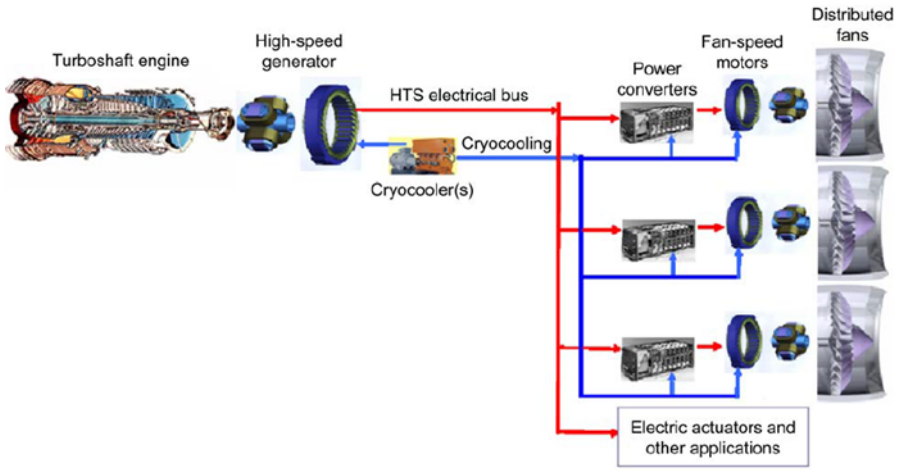

Figure 7: Components in a superconducting transmission system[10]

Some of the main merits and challenges of superconductivity are:

Merits

-Higher power to weight ratio compared to mechanical transmission of power.

-Decoupling of the propulsive device from the power-producing device enabling them to be positioned at their optimum locations.

-The speed of the power turbine shaft in the turbine engine is independent of the propulsor shaft speed, essentially the electrical systems acts as a gearbox with an arbitrary gear ratio.

Challenges

-The weight increase due to electrical equipment (motors, generators, transmission lines)

-System complexity due to additional new technology

-Cooling required to sustain very low temperatures required by the superconducting materials

In addition to the electrical system being feasible, it must be of adequate size and weight in order to result in fuel savings. The TeDP system adds the weight of motors, generators, inverters, power electronics and transmission lines. Simultaneously, it eliminates the need for a mechanical gearbox and it reduces the weight of the engine nacelles and pylons and also that of the propulsive system by being more fuel effective. The cooling of the electrical system is also a source of weight, losses and complexity. The low temperatures (less than 100K) required to maintain superconductivity can be achieved either by liquid hydrogen cooling or with a cryocooler which is a refrigerator that can produce very low temperatures. Overall, we can say that the weight of the electrical equipment is probably the biggest uncertainty for the viability of the TeDP system.

2.7 Thrust-Split

Cranfield University is actively involved in the field of DP and it has developed a conceptual framework to simulate and assess the performance of the TeDP vehicle from a TERA perspective. One of the innovations of Cranfield University is the use of the Thrust-Split (TS) [41] design parameter to characterise a TeDP configuration. TS is defined as the ratio of the thrust produced by the distributed propulsors to the total amount of thrust produced and it was introduced as a way to control the weight of the electrical system. By using TS, the prime movers which are the core-engines are not only used to provide power to run the distributed fans but also to produce some of the thrust of the aircraft. Producing less thrust from the distributed propulsors fans means that they require less electric power and hence the weight can reduce. Accordingly, the weight of the cooling system is also reduced and this is very important because the weight of the superconducting/cooling equipment is one of the biggest sources of uncertainty concerning the TeDP system and has a great impact on its viability. On the other side, the weight of the core engines is increased. NASA currently produces all the thrust from the Distributed Propulsors which effectively means they use a 100%TS.

2.8 Cooling technology

The High Temperature Superconducting (HTS) material lose their electrical resistance at a very low temperature (20 to 60 K) to remove the waste heat from the power transferring components, several solutions have been proposed[18]. The main cooling solutions examined are by using a cryo-cooler or by using LH2.

2.9 Weight estimation methods

Several methods from the public domain were reviewed, in order to establish the most suitable method for this research. Broadly these can be categorised in whole engine based approaches and component based approaches and the ones looked at, are:

Whole engine approaches:

- Single equation methods
- Clavier method
- Gerend and Roundhill method
-

Component based approaches:

- NASA WATE method
- Sagerser method

Single equation models are very simple and easily employed, but they lack the necessary accuracy. They are based usually on empirical or historical data and the engine weight data points are fitted with a linear correlation, some of them can be seen in Table 2Table 2.

Method	Weight correlations	Parameter
Whitehead and Brown (1953)	$WT = f\,(W_{des})^{1.45}$	W_{des} = Design mass flow
Pennington (1959)	$WT = f\,(Fn)^{1.5}$	Fn = Thrust
Svoboda (2000)	$WT = 250 + 0.175xFN_{to}$	FN_{to} = Take-off thrust

Table 2: Weight estimation methods

Clavier [29] linked the weight of the engine to a parameter which is a function of thermodynamic properties (Parameter = OPR^2 x BPR x MassFlow) and the curves in Figure 8 were produced.

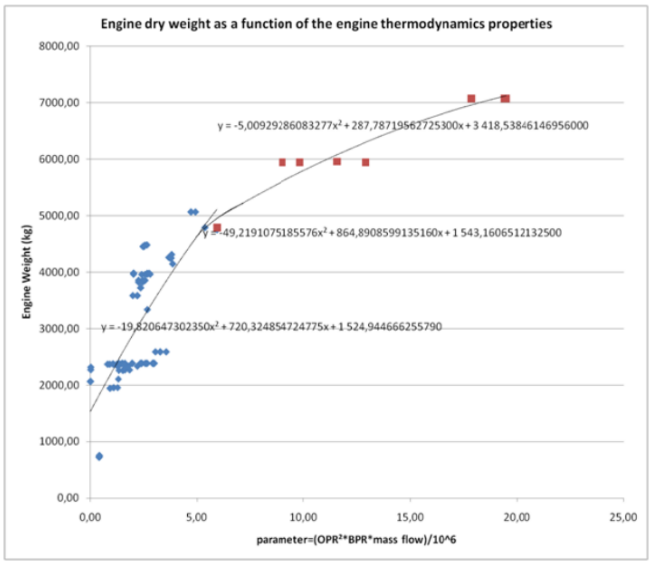

Figure 8: Engine weight estimation with Clavier method[29]

This method benefits from few inputs that can be inserted directly. On the other hand, this methods suffers from the lack of important variables and, as the author mentioned, large Parameter values resulted in negative weight.

Gerend and Roundhill [22] produced a method that used semi-empirical correlations to estimate preliminary weights for the entire propulsion system based on data for over 350 engines spanning from 1940 to 1980. This method used main cycle parameters (PR,BPR, TET,..) taken from diagrams, design flight Ma, and technology level to correct the weights.

In the NASA WATE method [50], the engine weight is obtained from the addition of each component weight calculations which are based on a set of correlations calibrated using historical data. This method is quite analytical and claims to offer an accuracy of 5%. The main disadvantage is that it requires many input parameters which leads to increased complexity.

Finally, the method that was used in this thesis is based in the Sagerser method [53]. This method was one of the first to calculate each component's weight and

dimensions separately. Even though the method was initially conceived for Vertical Take-Off and Landing engines (VTOL), it can be also used for cruise engines with some restrictions. The method provides simplified correlations for the fan, compressor, combustor and turbine. Additionally, it takes into account the weight of the controls and accessories and the structure. The correlations are based on geometrical data which are available after the basic preliminary design prepared using engine thermodynamic data. The authors claim to achieve an accuracy of +-10% but this is doubtful since the method was developed in 1971 and doesn't capture the newest technology.

2.10 Liquid Hydrogen

This part deals with the hydrogen used aboard an aircraft. Assuming that, in the long run, hydrogen will be produced from renewable energy, a transition to hydrogen has the potential to offer fuel burn benefits. The growth of the commercial aviation together with the increase in fuel demand by 3% per year in a "business as usual" approach calls for either increased specific fuel consumption either alternative fuels. Hydrogen presents a worthy alternative by being an energy carrier with ample abundance in the biosphere.

Hydrogen is 2.8 times lighter than kerosene but it occupies around 4.2 times the volume of a jet fuel of the same amount of energy as can be seen in Figure 9. This implies that a notable tank size is expected.

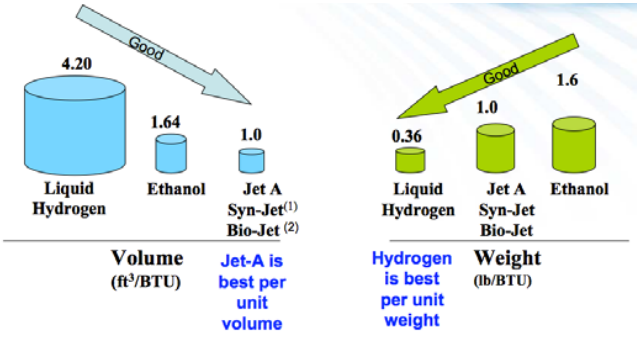

Figure 9: Volumetric and Gravimetric Comparison of Hydrogen per Calorific Equivalent Jet-A Fuel [1]

The combustion of hydrogen causes oxides of nitrogen (NOx) and water (H_2O). This gives a comparative advantage to hydrogen over hydrocarbon fuels as all carbon emissions that contribute to global warming are eliminated. However, water emissions that are elevated by a factor of 2.6 can also be regarded as greenhouse gases as they have an impact in the formation of contrails and cirrus clouds.

This thesis uses a preliminary size estimation of the hydrogen tanks, together with all safety measures that will be required in order to be incorporated in a TeDP vehicle.

3 METHODOLOGY

This section contains the procedures and methodologies that were used to simulate the different configurations and to achieve the performance assessments.

Throughout this thesis, several different aircraft configurations were used that correspond to different airframe, propulsion system and fuel type. These are summarized in figure 10.

Aircraft configuration	Definition
B777	Boeing B777-200 LR used for baseline comparisons
N3-A	BWB aircraft with 2 UHBPR podded geared turbofan engines and Kerosene
N3-X	BWB aircraft using embedded distributed propulsors powered by 2 turbofan engines and Kerosene
N3-X-L	BWB aircraft using embedded distributed propulsors powered by 2 turbofan engines and 100% LH_2 as fuel
N3-X-TS	BWB aircraft using embedded distributed propulsors powered by turbofans in order to employ the Thrust-Split variable

Figure 10: A summary of the configurations employed

3.1 Engine performance model

The engine performance model that was used in conjunction with the aircraft performance model is TURBOMATCH, Cranfield's in-house gas turbine simulation and assessment software. As mentioned earlier, TURBOMATCH was used to simulate the ge90-115b engine for the B777-200LR and turbofan engines to power the N3-A and N3-X conceptual aircrafts.

3.1.1 Ge90-115B engines (B777-200LR)

To power the B777-200LR aircraft, TURBOMATCH was used to simulate a two spool high bypass engine similar in design characteristics to the GE 90-110B15. The available data on the GE90-110B15 engine was limited to its take-off thrust (115,300 lbf or 514 kN), bypass ratio (8.8) and overall pressure ratio (42.9:1). The rest of the data is tentative and is assumed on the basis of previous GE90 engines with the appropriate improvements considered. The design point of the engine model was chosen at the take-off (i.e. sea level standard (SLS), Mach Speed 0.25, and the pressure recovery of 0.99 under International Standard Atmosphere (ISA) conditions. With TURBOMATCH, several iterations were completed at design and off-design point conditions to match the performance of the model with data obtained from the public domain for the engine on which the design was based. A summary of this data is presented in Table 3.

Ge-90-115B			
	Take Off Condition (Design Point)		Cruise Condition (Off Design Point)
	Literature[2; 14]	TURBOMATCH model	TURBOMATCH model
Altitude	0	0	9144
ISA		27	0
Mach Number		0.25	0.84
Thrust N (lbs)	514000 (115000)	514000	321740
TET		1831	1732

Mass Flow kg/s (lb/s)		1625	791
Fan PR		1.49	1.52
Bypass Ratio	8.8	8.8	8.7
IPC PR (Booster)		1.28	1.27
HPC PR		22.5	23.6
OPR	42.9	42.9	45.5
TSFC mg/Nsec (lbm/hr/lbf)		10.04 (0.355)	16.3 (0.576)
Fan Diameter m (inch)		3.25 (128)	3.25 (128)
Compressor pol eff		0.9325	0.9325
HPT		0.93	0.93
FPT		0.924	0.924

Table 3: Comparison of design and performance data of simulated engine with public domain

3.1.2 Turbofan engines (N3-A & N3-X)

For the N3A and N3X configurations, a turbofan engine was used as can be seen in figure 11. The only differences between the two turbofans is that the one used for the N3-A configuration powers purely a turbofan while the turbofan used for the N3-X configuration powers additionally the distributed propulsors through an electrical system.

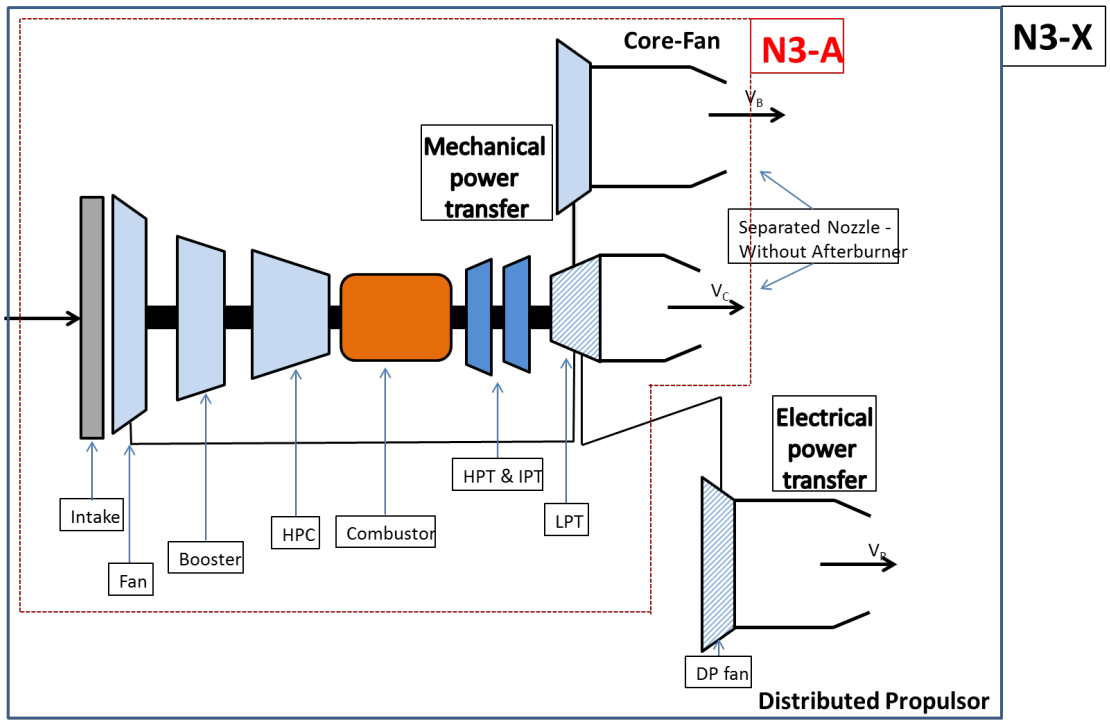

Figure 11: Turbofan engine configurations for the N3-A and N3-X configurations

3.2 Distributed propulsor model

In the past, several studies have considered and developed the modelling of the propulsor performance with BLI. In order to account for the effects of BLI and incorporate them into performance assessments, these methods depend on the control volume assumed. The method used in this study is based on the internal volume method, presented in section 2.5 and further explored in ref [35].

In this thesis, the benefits of BLI are captured through a reduction in the ram drag. For both embedded and podded engine installations, the total drag of the aircraft is considered identical leading to a similar net thrust. However, in the case of the embedded engines, the ram drag is reduced due to the lower momentum fluid ingested. Therefore, the gross thrust of the aircraft using BLI will be lower and this will provide fuel benefits.

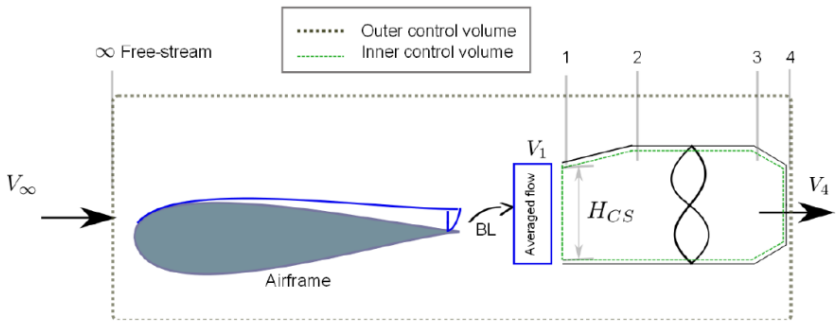

Figure 12: Propulsor scheme [59]

The reduction of the ram drag is addressed by using a Mach number lower than the free stream value in the MATLAB code (described in 2.5) that calculates the required power by the distributed propulsors. So, the benefit of BLI is translated into a reduction of the power requirements of the distributed propulsors. This method requires the inlet BL properties to be known and these have been adapted from those available for the N3-X concept [20]. The induced distortion was taken into account with a 1% penalty in the fan efficiency and 1% in the intake pressure losses.

For the performance calculation of the distributed propulsors, a 1-D momentum based method using the internal control volume shown in figure 12 is utilized. The design point used is the ADP (Aerodynamic Design Point). The intrinsic net thrust using this control volume is defined as follows:

$$F_N = NF\ (m_f(V_4 - V_1) + (p_4 - p_1)A_4 - (p_1 - p_\infty)A_1)\ , \quad (1)$$

where:

- NF represents the number of distributed fans used for propulsion
- p_{oo} is the static pressure at free stream conditions
- A_1 is the inlet capture height and p_1 the inlet static pressure
- A_4 is the exit nozzle area
- p_4 is the exit nozzle static pressure.

- V_1 is the inlet velocity, which is reduced from the freestream value due to BLI
- U_4 is the fan exit velocity
- m_f is the mass flow of a single fan

To account for the reduction in momentum drag due to BLI, the control volume inlet properties are assumed equal to the BL properties mass averaged values. These values were calculated based on the BL profiles provided in [20], which are assumed at a distance of x/c = 0.85 as can be seen in figure 13.

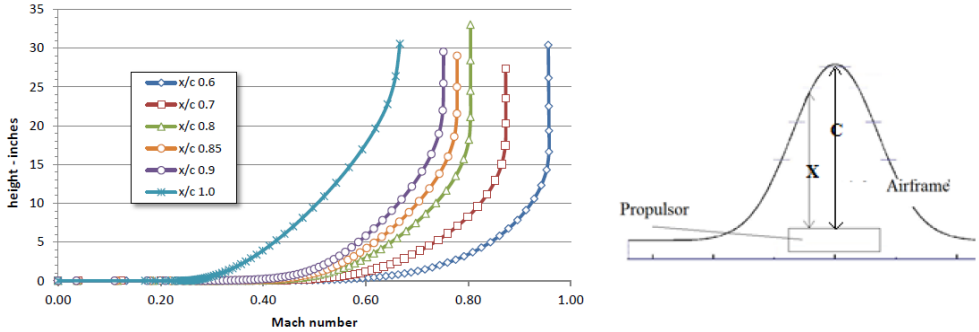

Figure 13: Distributed Propulsor inlet properties

To simplify the analysis, the inlet control volume (station 1 - figure 12) is located at this position (x/c = 0.85) and is assumed that the ingested BL has not been either diffused or compressed within the stream tube entering the intake [35] . In other words, it is assumed that at design point the height of the intake is equal to the height of the capture sheet.

In order to define the height of the BLI, the capture sheet height is utilized as the handle in an iterative calculation. The capture sheet height is calculated assuming a mailbox intake of width equal to the fan diameter and using continuity equation. Figure 14 depicts a schematic diagram of the intake configuration. The space available to allocate the propulsors (23 m) is set and therefore depending on the propulsors diameter the separation (S_{in}) between them may be calculated. To calculate the fan hub diameter a root to tip ratio of 0.52 is assumed and this is based on the NASA stage 53 [48], which uses a fan

stage operating at similar conditions. A 0.6 Mach number was assumed at the fan face.

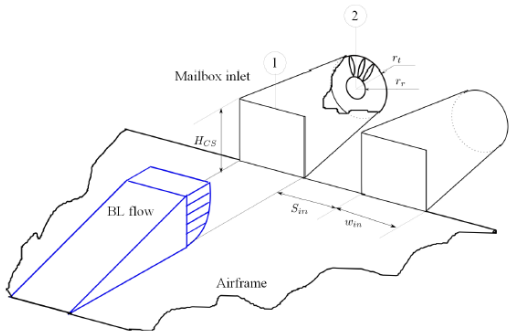

Figure 14: Propulsion airframe integration [59]

In this propulsor assessment, the fan pressure ratio is an input variable and the design is based from ref [20], where the fan efficiency and fan tip speed are given for a range of pressure ratios. To calculate the flow properties at the exit station, a nozzle pressure loss of 1 % is assumed. Finally, using equation 1 and the exit flow properties the mass flow of the propulsors is calculated iteratively using the intrinsic thrust as the required matching condition. As the propulsor need to deliver the intrinsic thrust for all the configurations, the pressure ratio defines the mass flow and hence the capture sheet height for each configuration. The inputs and the outputs of this model can be seen in table 4. A more detailed description of the method used for the distributed propulsor assessment can be found in [59].

Inputs	Outputs
Fan pressure ratio	Power required by the propulsors
Fan efficiency drop due to BLI	Mass flows
Intake pressure losses due to BLI	Propulsor diameter

Number of fans	
Propulsor array width	
Thrust Split ratio	
Mission Parameters (Ma, alt)	
Net Thrust required	

Table 4: Input and output parameters of the power requirement model

3.3 Aircraft configurations modelling

3.3.1 B777-200LR

The reference data for the 300 passenger Boeing 777 have been taken from the Jane's "All the world's aircraft" [30] and from the B777-200LR Airport Planning Manual [9]. Geometric data was measured from the top-view drawing. The B777-200LR layout and geometry were acquired from publicly available data and they were converted into geometric data for input into FLOPS. These values, together with assumed parameters, can be seen in Table 5.

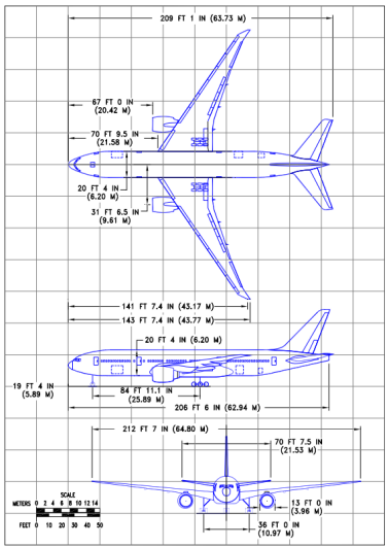

Figure 15: Drawings of the B777-200LR

FLOPS parameter	Description	Value	Units
SW	Wing area	450 (4843)	m^2 (ft^2)
SPAN	Wing span	64.8 (212)	m (ft)
AR	Wing Aspect Ratio	9.34	-
TR	Wing Taper ratio	0.163	-
SWEEP	Wing ¼ chord sweep angle	25	°
XL	Fuselage total length	204	ft
SPAN	Wing Span	212	ft
DESRNG	Design range	7500	nm
WSR	required wing loading	167	

TWR	required total thrust-weight ratio	0.287	
TCA	Wing thickness-chord ratio	0.1	
CH	Maximum cruise altitude	40000	ft
AITEK	Airfoil technology parameter	2	

Table 5: Aircraft Geometric Input for NASA FLOPS Aircraft Analysis Tool

Based on public data [9], take-off and landing distances of 3350m and 1676m were taken respectively and an approach speed of 140 kt (72 m/s) was also assumed. Some of the additional FLOPS mission inputs are shown in Table 6.

FLOPS parameter	**Description**	**Value**	
NPF	Number of first class passengers	20	
NPT	Number of tourist class passengers	280	
VCMN	Cruise Mach number	0.84	
NTABR	Number of tourist class passengers abreast	7	
NFABR	Number of first class passengers abreast	6	
FWF	Climb profile optimization function control parameter	(minimum fuel-to-climb profile) -1	
IRS	Reserve fuel	(Reserves at	

	calculation switch	constant values) 2	
RESRFU	Contingencies	(Reserve fuel as a fraction of total usable fuel weight) 0.05	
ALTRAN	Range to alternate airport	200	nm
THOLD	Reserve holding time	20	min

Table 6: Aircraft mission parameters

3.3.2 UHBPR Blended-Wing-Body with podded engines (N3-A)

The N3-A concept is a Blended-Wing-Body conceptual aircraft with Ultra High Bypass Ratio. It is used in order to distinguish the performance benefits due to the higher effective bypass ratio and due to the benefits of using BLI.

The mission profile used for all the configurations is the same although improved ground and air management systems in the future may allow reduction of idle times, removal of time and distance to climb requirements and could offer more potential improvements. The mission profile used for all the configurations consists of a climb, cruise, descent, and reserve segment.

A general guideline followed was to choose the same baseline configurations and main design parameters as in NASA references [17; 21] in order to make more accurate comparisons. The weights and block fuel values that were targeted [17] in order to match the baseline configurations can be seen in Table 7. All the configurations performed a mission of 7500 nm range (13890 km) with a cruise speed of Mach 0.84 and an 118100 lb payload.

	B777-200LR	**N3-A**	**N3-X - LH_2 cooled**	Units

Empty Wt	340800 (154584)	285800 (129635)	267400 (121290)	Lb (kg)
Payload Wt	118100 (53569)	118100 (53569)	118100 (53569)	Lb (kg)
Total Fuel Wt	309800 (140522)	147200 (66768)	88000 (39916)	Lb (kg)
Block Fuel Wt	**279800 (126915)**	**133700 (60645)**	**78500 (35606)**	**Lb (kg)**
TOGW	768700 (348676)	551000 (249929)	473500 (214775)	Lb (kg)

Table 7: Performance goals targeted

3.3.3 Blended-Wing-Body with embedded engines (N3-X)

This chapter describes the way that the baseline N3-X configuration was modelled. The results from all the N3-X simulations are included in chapter 4. The methodology used to model the N3-X can be seen in figure 16. The power required (section 3.2), an engine deck (3.3.3.1), the weight (3.4) were inserted in the aircraft performance model (3.5) that was used to calculated the performance.

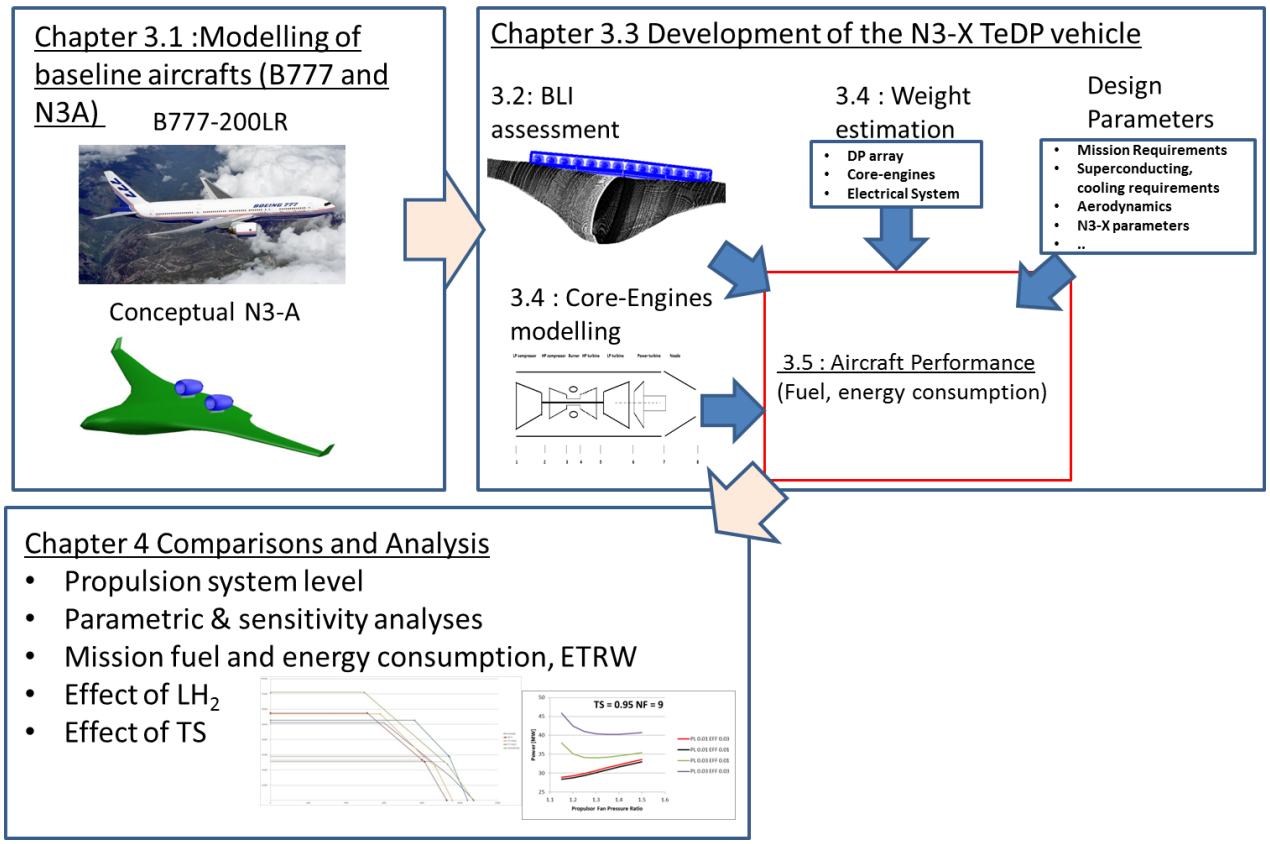

Figure 16: N3-X methodology

3.3.3.1 Engine deck creation

Turbomatch was used to create an engine deck consisting of thrust and fuel flow data at a variety of Mach-altitude conditions. This was introduced in FLOPS to model the propulsion system. The steps used for the creation of the engine deck are :

1. Use BLI assessment tool (3.2) to obtain power required by Distributed Propulsors
2. Use Turbomatch to match the uninstall thrust at ADP, RTO and the power required
3. Add the thrust of the Distributed propulsors
4. Obtain the engine deck and input to FLOPS

3.3.3.2 Configuration and assumptions

For this study of the N3-X configuration, the N3-A airframe was used with some differentiations. The main difference is the use of embedded distributed propulsors powered by core-engines instead of using podded engines.

The fuselage length was chosen 133 ft (40.5 m) and the span 200 ft (90.9 m). The wing geometry was input in FLOPS through a positive value of input stations (NETAW), wing stations (ETAW), chords (CHD), t/c's (TOC) and sweeps (SWL) defined at wing root, break points and tips.

For the baseline version of the N3-X, 15 propulsors were chosen with a 1.3 FPR. All the propulsors were assumed to be positioned at the upper rear airframe at a distance of 85 % of the centreline inside an array. The array has a length of 75.4 (23 m) and the height was allowed to vary according to the propulsor assessment model. The fan tip speed and adiabatic efficiency were adapted from a reference from NASA [20].

3.3.3.3 Core-Engines and Thrust Split implementation

As was mentioned before for all the N3-X configurations, two turbofan engines were used with a power turbine mounted in the low spool shaft instead of two turboshaft engine. Part of the thrust is produced by the distributed propulsors and the rest from the main and bypass nozzles.

To achieve the baseline N3-X configuration and match the performance targets, the same engine and component parameters as in ref [17] were used as can be seen in table 8 and 9.

Parameter	Value	
	3-spool Turbofan	
	ADP	RTO
Altitude ft (m)	30000 (9144)	0
M	0.84	0.25
Pt	6.93	15.35
By pass ratio	Variable	Variable
Fan pressure ratio	Variable	Variable
Overall Pressure ratio	64	55.8
Turbine Inlet temperature	1693	993

Table 8:N3-X turbofan engine parameters

The uninstalled thrust required by the N3-X is 54888 lbf (244 kN) at RTO and 19293 lbf (85.82 kN) at ADP [17]. The ADP was chosen as the design-point in order to size the electrical system at lower demanding conditions.

Components	Parameter	Value
LP & HP	Polytropic efficiency	0.9325

compressors		
HP compressors	Maximum exit total temperature (T3)	
LP & HP compressors	Pressure ratio	OPR varied to equal max T3 with equal Δh split between compressors
Burner	Exit total temperature (T4)	
	Efficiency	0.998
	Pressure losses	3.5 %
HP & LP turbines	Polytropic efficiency	0.93
Power turbine	Polytropic efficiency	0.924

Table 9: N3-X turbofan engine component parameters

When using a TS ratio, the creation of the engine deck is modified by changing the thrust required to match and the power required by the distributed propulsors.

3.3.3.4 Superconducting and cooling system

The turboelectric approach requires that a number of new electric components are inserted into the aircraft propulsive drive train between the core-engines and the distributed fans. For the N3-X these are the generators, motors, and transmission lines as a means of transferring power from the turbines to the fans. The overall system model can be seen in figure 18 where *W* is the power. The efficiency of the motor and the generator is assumed 0.9999 and the transmission efficiency 0.999.

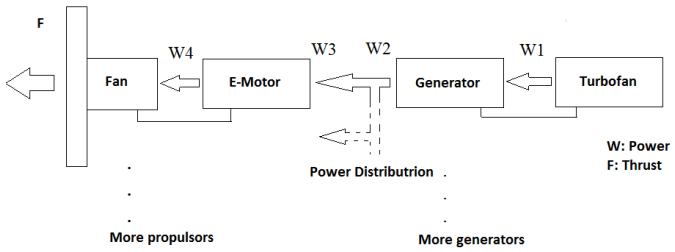

Figure 17: N3-X electrical components

$$W_2 = \mu_{generator} x\, W_1$$

$$W_3 = \frac{Num_T}{Num_F}\, \mu_{transmit} x\, W_2$$

$$W_4 = \mu_{e-motor} x\, W_3$$

The electrical system weight was calculated with the method described in 3.4.3. For the kerosene-fuelled configurations, the barium strontium calcium copper oxide (BSCCO) superconducting material was used combined with a cryocooler refrigerated system. For the LH_2-fuelled configurations, the magnesium diboride (M_gB_2) superconducting material was used while cooling was provided from the liquid hydrogen instead of a cryocooler. The weight of both electrical and cooling systems is calculated as provided in chapter 2.

3.3.3.5 FLOPS inputs

Some of the main parameters used in FLOPS can be seen in table 10.

FLOPS parameter	Description	Value	
NPF	Number of first class passengers	20	
NPT	Number of tourist class passengers	280	

VCMN	Cruise Mach number	0.84	
NTABR	Number of tourist class passengers abreast	6	
NFABR	Number of first class passengers abreast	4	
NEW	Number of wing mounted engines	0	
NEF	Number of fuselage mounted engines	2	
FCOMP	Decimal fraction of amount of composites used in wing structure	1	
FWF	Climb profile optimization function control parameter	(minimum fuel-to-climb profile) -1	
IRS	Reserve fuel calculation switch	(Reserves at constant values) 2	
NETAW	Number of input wing stations	i=7	
SW	Reference wing area	9246	sq ft
ETAW(i)	Wing station location	Appendix B	
CHD(i)	Chord length	Appendix B	
TOC(i)	Thickness - chord ratio	Appendix B	
SWL(i)	Sweep of load path	Appendix B	
AR	Wing aspect ratio	7.5	

TR	Wing taper ratio	0.311	
SWEEP	Wing ¼ chord sweep angle	0.36	
RESRFU	Contingencies	(Reserve fuel as a fraction of total usable fuel weight) 0.05	
ALTRAN	Range to alternate airport	200	nm
THOLD	Reserve holding time	20	min

Table 10: Main N3-X parameters used in FLOPS

3.4 Weight estimation model

The model employed calculates the weight of the following three subsystems:

- Core-engines weight
- Distributed propulsors
- Electrical system
- Cooling system

These subsystems constitute the propulsion system weight although several components were not taken into account such as variable geometry mechanisms, acoustic linings bearings and more. The weight model received input from other TURBOMATCH (i.e. mass flows, temperatures, pressures) and the propulsor assessment model (i.e. propulsor mass flow and power requirement of motors and generators).

3.4.1 Core-engines

The weight model used for the core-engines is based on the empirical relationships available from Sagerser [53] that calculates each component's

weight separately. The weight of the core-engines consists of the fan, the compressors, combustors and turbines. A step-by-step explanation of the steps used in this analysis to calculate each component is placed in Appendix A.

3.4.2 Distributed Propulsor

The weight of the distributed propulsor array consists of the fans, the ducts and electrical generator. For the fan and ducts, the equations used are the same as the ones for the fan of the turbofan, based on Sagerser [53]. The weight of the motors is included in the superconducting equipment section.

3.4.3 Electrical system

This weight of the superconducting equipment is based on the chart in Figure 19 presented by Felder [19]. The red dotted line represents a trend line approximately valid for all the high temperature superconducting equipment. By using the power demand from the power model, the weight can be estimated.

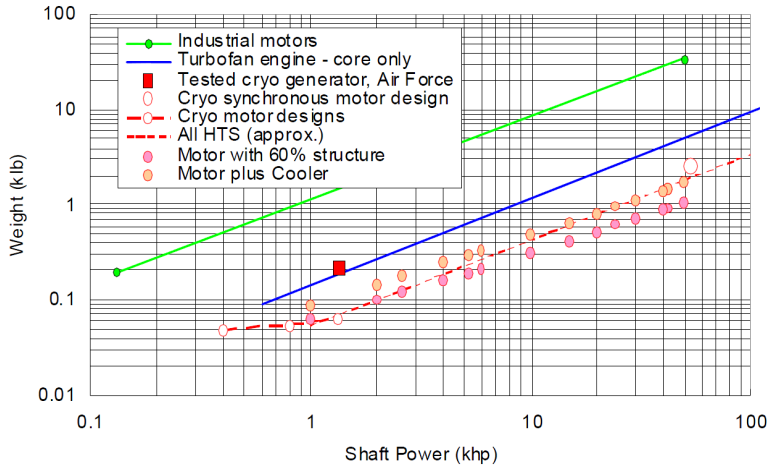

Figure 18: Preliminary electric system weight estimation [19]

The curve has been implemented by using equation (2) for P < 1 khp and equation (3) for P > 1 khp:

$$logW = \frac{\log 0.06 - \log 0.05}{\log 1 - \log 0.4} (\log P - \log 0.4) + \log 0.05 \quad (2)$$

$$logW = \frac{\log 3 - \log 0.06}{\log 90 - \log 1} (\log P - \log 1) + \log 0.06 \quad (3)$$

3.4.4 Cooling system

For the N3-X configurations that used kerosene as fuel, cooling through a cryocooler was assumed and a weight was added equal to the 70% of the weight of the electrical system.

For the LH_2-fuelled configurations, LH_2 cooling was assumed and hence no added weight for refrigeration was needed. The size and weight of the LH_2 tanks was considered as part of the propulsion system weight and the methodology is described in the next section. Considering the weight for the transmission lines and inverters from [11], the total weight of the electric equipment can be obtained.

3.4.5 LH2 tanks

The procedure used to calculate the weight of the LH2 tanks was adapted from [39]which was based on [10; 56].For the cases where LH2 was used as a fuel, an additional weight due to the weight of the tanks was calculated. Concerning the on board storage, a cylindrical geometry with hemispherical end caps was used because of its higher volumetric efficiency and optimum space usage. The required inputs of the model are:

- Mass of LH_2 to be stored (calculated from FLOPS) ,M_H (kg)
- Operating pressure inside the tank, P (Pa)
- Temperature, T (K)

- Density of LH_2, ρ (kg/m^3)
- Excess volume to maintain pressure and for boil-off, V_i (%)
- Length of the tank, L (m)
- Aluminium yield strength, σ_y = 80 MPa
- Factor Of Safety, FOS = 1.5

The required tank volume (V_t), to hold a given mass of hydrogen is calculated with the following equation:

$$V_t = \frac{M_H(1+V_i)}{\rho_{LH}} \qquad (4)$$

Once the volume is known, the tank radius, r, is then calculated by:

$$V_t = \frac{4\pi r^3}{3+(\pi r^2 L)}, \qquad (5)$$

The tank wall thickness is then calculated by:

$$t_w = \frac{P\ r\ FOS}{2\ \sigma_y} \qquad (6)$$

The mass of the LH_2 tank is calculated by the following equation:

$$M_t = \rho\ \left[\left(\frac{4\ \pi\ (r+t_w)^3}{3}\right) + \pi(r+t_w)^2 L - V_t\right] \qquad (7)$$

Finally, the estimation of the boil-off mass and the material of the insulation is placed in Appendix B. The weight of the tanks was calculated based on the fuel burn and then it was added without optimisation. The LH2 tanks were bookkept as part of the propulsion system and so as the amount of hydrogen increases so too does the propulsion system weight.

3.5 Aircraft performance model

3.5.1 FLight OPtimisation System (FLOPS)

The mission performance was performed using FLOPS[46] which is a multidisciplinary system of computer programs for conceptual and preliminary design and evaluation of advanced aircraft concepts. It consists of several

modules and, among others, it is able to estimate the drag using the “Empirical Drag Estimation Technique” [16], the weight of the aircraft using the WATE method and the performance which is based on a point-mass method and energy considerations.

3.5.2 Metrics

3.5.2.1 Payload-Range chart

The payload-range chart is an important tool used for assessment and decision making, during the process of selecting an aircraft or fleet. It shows the maximum allowable revenue generating payload that can be carried by a particular aircraft.

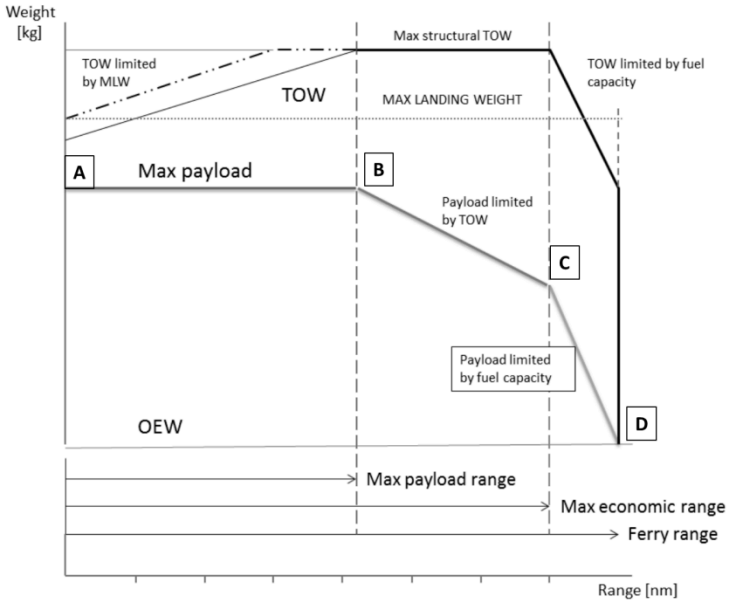

Figure 19: Typical payload-range chart

A payload-range chart effectively consists of four critical points (as seen in Figure 20). The first point (A) shows the maximum volumetric payload that can be carried by a specific aircraft, while respecting the structural limitations. Point B represents the maximum range that can be achieved by the aircraft while respecting the Maximum Take-Off Weight (MTOW). Point C represents the range that is achieved with maximum fuel on board and the payload is reduced

so that the aircraft is still at MTOW. Point D shows the ferry range that is achieved with zero payload.

3.5.2.2 Energy To Revenue Work (ETRW) ratio

This thesis also utilised the *Energy to Revenue Work* (ETRW) ratio as a metric to assess a technology purely from an energy efficiency perspective[4]. The metric analyses the amount of productivity in terms of payload transferred across a distance per unit cost of energy consumed. It can be also be employed as a key indicator to assess the environmental impact and hence has been found particularly useful in comparing two competing transportation technologies. The minimum value of this metric is considered as the optimal value in terms of energy efficiency and is calculated as follows:

$$ETRW = \frac{revenue\ work\ done}{cost\ of\ energy\ use} = \frac{M_f LCV}{M_{pl} gR}$$

Where M_f is the mass of the mission fuel actually burned on trip (kg), M_{pl} is the maximum payload mass of the aircraft (passenger+ cargo) (kg), g the acceleration due to gravity (9.81 m/s2), R the Great circle distance for a mission (m) and LCV the Lower calorific value of fuel (≈ 43 MJ/kg for kerosene, 120 MJ/kg for LH_2).

4 RESULTS

4.1 Baseline configurations matching

4.1.1 B777-200LR

The B777 aircraft and ge90-115B engine model were integrated and a series of validation tests were performed to validate/verify the performance of the models with the help of the payload range chart. The payload-range diagram (figure 20) delivers the combinations of payload and range listed in Table 11.

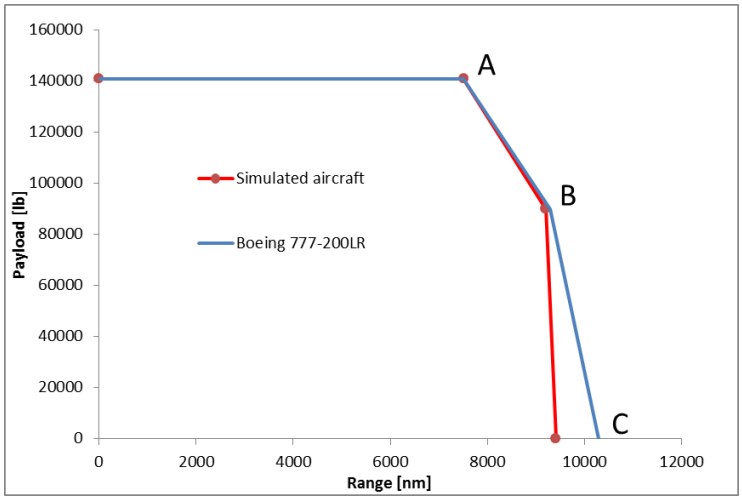

Figure 20: Payload range validation of the B777 configuration

	Max Payload range (A)	Max fuel range (B)	Max ferry range (C)
Cruise Mach Number	0.84	0.84	0.84
Altitude at cruise ft	35000	35000	35000
Maximum Take-off	347452	347452	290638 (640747)

weight kg (lb)	(766000)	(766000)	
Maximum payload kg (lb)	64000 (141000)	40800 (89900)	0
Operating empty weight kg (lb)	145100 (320000)	145100 (320000)	145100 (320000)
Maximum fuel on board kg (lb)	138352 (305000)	145538 (320800)	145538 (320800)
Reserves fuel (hold + diversion + contingencies) kg (lb)	(27798)	(29450)	(14750)
Fuel consumption kg (lb)	(277000)	(327000)	(295000)
Range Calculated in FLOPS nm	7513	9198	9413
Range Boeing 777-200LR nm	7500	9300	10300
Range error %	**0.15 %**	**1%**	**8.6%**

Table 11: Payload range validation of the B777 configuration

An additional simulation was performed to match data from NASA reference [17] and the results can be seen in table 12.

	Baseline 777	Calculated 777	Difference
Empty lb (kg)	340800 (154584)	Same	
Payload lb (kg)	118100 (53569)	Same	
Total Fuel lb (kg)	309800 (140522)	Same	
TOGW lb (kg)	768700 (348676)	Same	
Block Fuel lb (kg)	**279800 (126915)**	**278722 (127800)**	**0.6%**

Table 12: B777 Performance validation

4.1.2 N3-A

The goal of modelling was to aim to achieve the performance goals published by NASA [17] and the results/comparisons can be seen in table 13.

	ADP	ADP	RTO	RTO
	N3-A engine	**simulated N3-A engine**	**N3-A engine**	**simulated N3-A engine**
Altitude ft (m)	0	0	30000 (9144)	30000 (9144)
Mach number	0.25	0.25	0.84	0.84
dTs R (K)	27 (15)	27 (15)	0	0
ambient Pt psi (atm)	15.35 (1.04)	13.5 (0.92)	6.93 (0.471)	6.75 (0.46)
capture MN psi (atm)	0.25	0.25	0.84	0.84
capture Pt psi (atm)	15.35 (1.04)	13.5 (0.92)	6.93 (0.471)	6.75 (0.46)
T3 R (K)	1803 (1001)	1803 (1001)	1670 (927)	1661 (923)
T4 R (K)	3360 (1866)	3474 (1930)	3212 (1784)	3212 (1784)
Uninstalled Fn lbf (kN)	**78766 (350)**	**77780 (346)**	**25378 (112)**	**25402 (113)**
Wfuel lb/hr (kg/s)	**20177 (2.54)**	**20671 (2.61)**	**11281 (1.42)**	**11721 (1.48)**
Uninstalled TSFC lbm/hr/lbf (g/kNs)	**0.2578 (7.3)**	**0.265 (7.54)**	**0.4667 (13.2)**	**0.462 (13.1)**
Wair lb/s (kg/s)	6539 (2966)	5403 (2456)	3485 (1580)	3485 (1580)

BPR	29.5	27.8	27.2	27.2
FPR	1.2	1.2	1.29	1.29
OPR	57.4	58.3	71.1	71.1
Vamb ft/s (kg/s)	286.3 (87.2)	282 (86)	835.8 (254.8)	835.8 (254.8)
Vcapture ft/s (kg/s)	286.3 (87.2)	282 (86)	835.8 (254.8)	835.8 (254.8)
Vbypass ft/s (m/s)	665 (202)	718 (219)	1006 (306)	1013 (309)
Fan Diameter in (m)	150 (3.81)	150 (3.81)	150 (3.81)	150 (3.81)

Table 13: N3-A performance results

An additional simulation was performed to match data from NASA reference [17] and the results can be seen in Table 14.

	Baseline B777-200LR	**Calculated B777-200LR**	**Difference**
Empty lb (kg)	285800 (129636)	Same	
Payload lb (kg)	118100 (53569)	Same	
Total Fuel lb (kg)	147200 (66768)	Same	
TOGW lb (kg)	551000 (249929)	Same	
Block Fuel lb (kg)	**133700 (60645)**	**130984.7(127800)**	**1.2 %**

Table 14: N3-A Performance validation

4.1.3 N3-X

The turbofan configuration used to model the baseline N3-X configuration was based on the parameters of table 13 and 15.

Parameter	Value
BPR	9
FPR	1.2
TET	1689

Table 15: N3-X baseline configuration parameters

The performance results for the baseline N3-X can be seen in table 16. The results are compared to the N3-X configuration that was presented in reference [17] . The difference of 12% can be attributed to several reasons. Using turbofans instead of turboshaft as core-engines increased the weight of the propulsion system whilst the total amount of uninstalled thrust required was the same. Also, many geometrical parameters were unknown and the assumption that the distributed propulsion power and thrust requirements were constant at off-design conditions must be refined.

	Baseline N3-X	Calculated N3-X	Difference
Empty lb (kg)	267400 (129636)	Same	
Payload lb (kg)	118100 (53569)	Same	
Total Fuel lb (kg)	88000 (66768)	Same	
TOGW lb (kg)	473500 (249929)	483000 (219085)	**2%**
Block Fuel lb (kg)	**78500 (35607)**	**88500 (127800)**	**12 %**

Table 16: N3-X baseline performance

4.2 Distributed propulsor assessment

The results corresponding to the propulsor performance model are shown in this section. The results are obtained considering the input data presented for the N3-X configuration at ADP conditions i.e. 30000 ft at Mach number 0.84 and for a uninstalled thrust requirement of 19293 lbf (85.82 kN).

Figure 22 shows the power demand of for a number propulsors (11, 14, and 17) of different FPR (1.1-1.45). Additionally for 14 fans, the effect of increasing the fan efficiency drop (EFF) and intake pressure losses (PL) from 1% to 3% is illustrated.

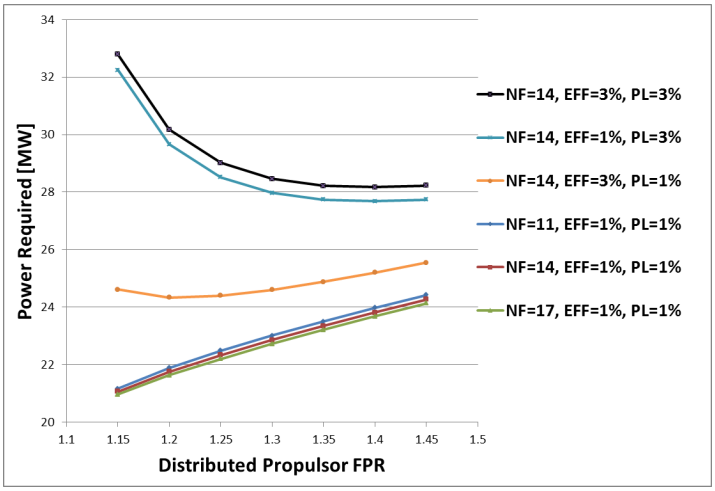

Figure 21: Power requirement analysis for different penalties at different number of fan

For a constant FPR, increasing the number of fans leads to a lower power requirement. This is because, in this analysis, the space allocated for the propulsors is fixed and using more propulsors increases the length covered by them and reduces the capture sheet height. A reduction in the latter translates in lower momentum drag and hence a reduction in propulsor's mass flow, which in turns results in a reduction in power consumed.

It has to be noted that the results are based on the assumptions that intake pressure losses are constant when different number propulsors of different FPR are used. Additionally, the fan efficiency degradation is constant and doesn't vary with the amount of flow ingested. The remaining figures in this section

show the weight of the distributed propulsors, electrical system, turbofans and the total weight of the propulsion system.

In order to calculate the benefit of BLI in terms of reduced power requirement of the distributed propulsors, a non-BLI configuration was modelled where it was assumed that the distributed propulsors ingested only free-stream air, similar to a podded configuration. Additionally, it can be seen that the relative BLI benefit increases as the installation losses are reduced.

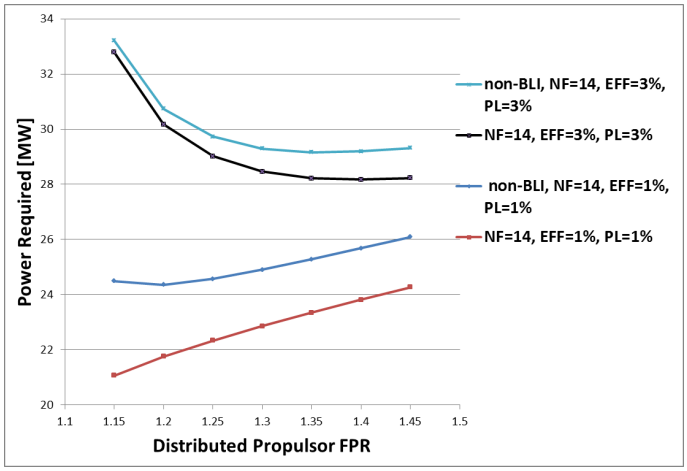

Figure 22: Power of superconducting equipment for different distributed propulsor FPR

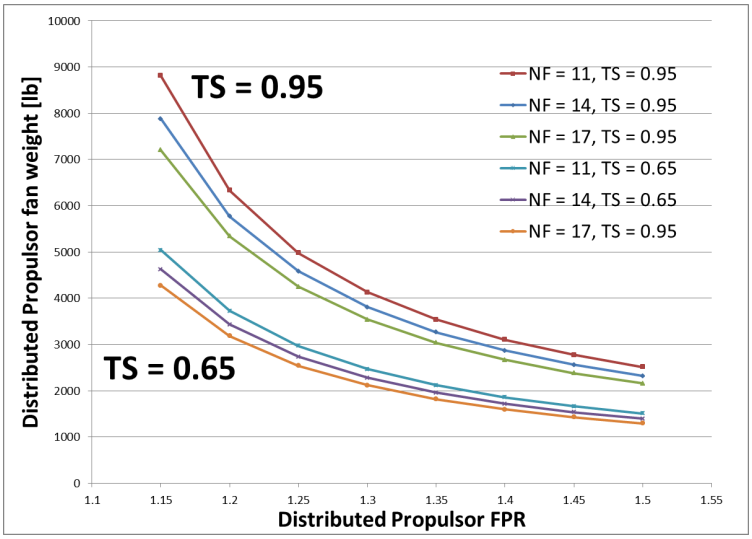

Figure 23: Distributed Propulsor fan weight for different FPR

Figure 25 shows the weight of the turbofan engines for several TS ratios. The trends can be explained keeping in mind that the weight estimation was performed for the optimum configurations in terms of SFC. For a constant BPR, the FPR was varied and this varied the number of stages which in turn has a big influence on the weight of the whole turbofan engine. The results show that for these conditions, a minimum configuration can be obtained by using a TS ratio of 65-70% for the case of BPR 4.

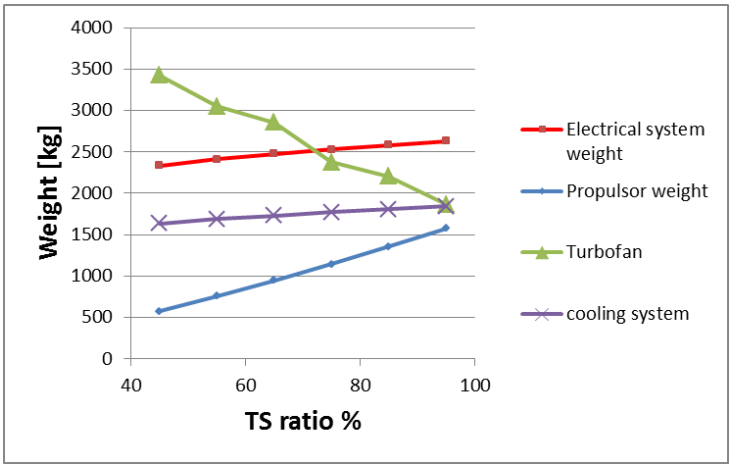

Figure 24: Weight of turbofan engines for different TS ratios

This figure shows that while the weight of separate components might display a minimum/maximum at a certain TS ratio, this might not be the case for the whole propulsion system.

4.3 N3-X aircraft mission performance results

For the remaining of the analysis, a specific distributed propulsion configuration was used and the parameters can be seen in table 17.

Parameter	Value
FPR	1.3
Intake pressure losses	1%
Fan efficiency drop	1%
Number of fans	14

Table 17: Distributed Propulsor parameters used for core engine analysis

The results in this section first show the mission fuel burn for the set of missions selected and for the three baseline configurations. On each mission both aircraft are assumed to be carrying a payload of 118100 lb. This payload has been selected as the common payload at which the capability of both aircraft can be compared. A summary of the fuel burn for the different missions of N3-X and relative changes when the B777 and N3-A are used is as illustrated in table 18 and figure 26.

Range (nm)	B777	N3-A	N3-X	%Improvement in fuel consumption	
	Fuel Burn (lb)	Fuel Burn (lb)	Fuel Burn (lb)	compared to B777	compared to N3A
7500	278722	130984	85862	69.2	34.4
7000	255549	121055	79667	68.8	34.2
6500	233168	111348	73568	68.4	33.9
6000	211678	101861	67566	68.1	33.7
5500	190771	92583	61654	67.7	33.4
5000	170589	83505	55831	67.3	33.1
4500	151096	74614	50094	66.8	32.9
4000	132259	65907	44439	66.4	32.6
3500	114034	57371	38865	65.9	32.3
3000	96421	49002	33368	65.4	31.9
2500	79366	40792	27947	64.8	31.5
2000	62866	32737	22599	64.1	31.0

Table 18: Estimated fuel burn over different ranges for the N3X (with 95%TS) and baseline configurations

As expected due to the fuel burn improvements, the payload range chart in figure 26 illustrates that with the N3-X the aircraft's range capability improves (illustrated by three key points on the payload range chart, figure 26). The range with maximum payload (point A) is the same as this was the target mission. The range flown with maximum fuel and associated payload to maintain maximum take-off weight (point B) has increased by 8%.The ferry range (point C) has increased by 14%.

As no data is available, a maximum take-off weight of 520850 lb and maximum fuel of 180000 lb were assumed.

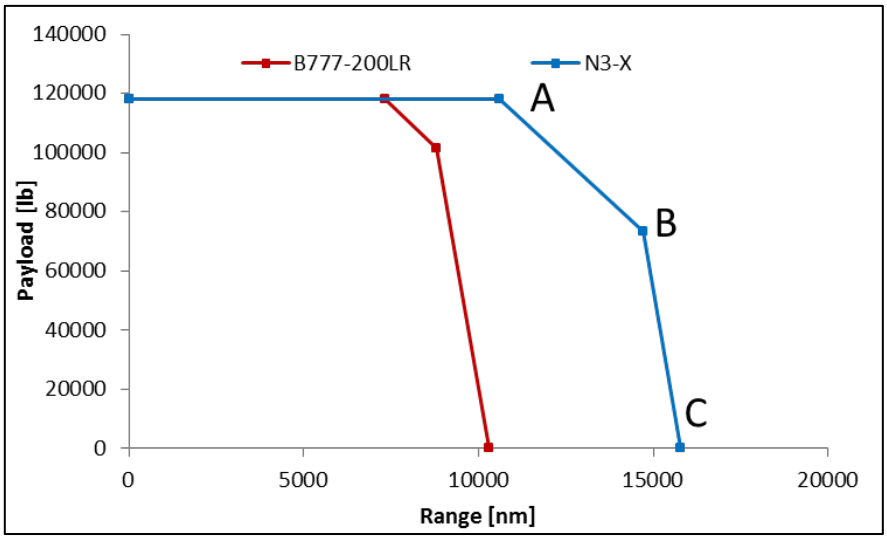

Figure 25: Payload-range chart for the N3-X and B777

For the target mission of 7500 nm, the N3-X shows a fuel burn improvement of 69.2% compared to the B777 and hence it shows that it has the benefit to achieve the “better than -70%” reduction goal for the N+3 timeframe. As can be seen in figure 26, the conventional B777 is less energy efficient amongst the 3 configurations in terms of ETRW. Also, it can be seen that, the N-3X is more efficient as the range of the mission increases. The same results can be identified in the ETRW chart in figure 28.

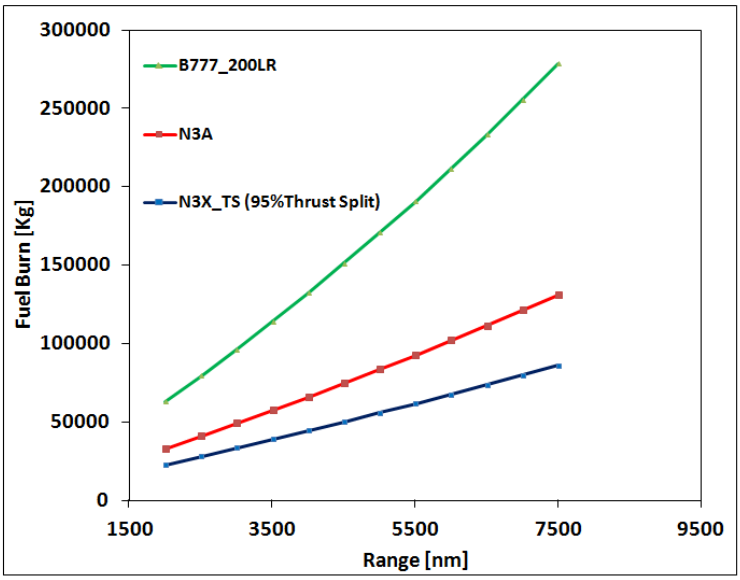

Figure 26: Estimated fuel burn over different ranges for the N3-X (95%TS) and baseline configurations

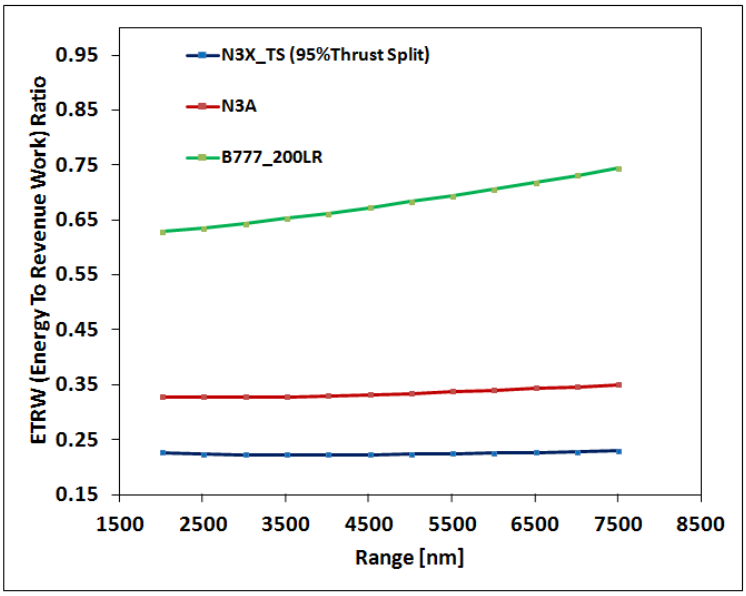

Figure 27: Energy efficiency curves over different ranges for the N3-X (95%TS) and baseline configurations

4.3.1 Comparisons with baseline aircrafts

4.3.2 N3-X with LH2

In this section the effect of changing the fuel from kerosene to purely LH_2 are assessed. Initially, configurations using LH2 (N3-X-L) and kerosene (N3-X) are compared using the ETRW parameter without taking into account the required volume for the LH_2 tanks, this is assessed separately. Figure 29 shows the ETRW parameter for a mission of constant range of 7500 nm. As the number of passenger is increased, the N3-X-L configuration provides increasing benefits compared to the N3-X.

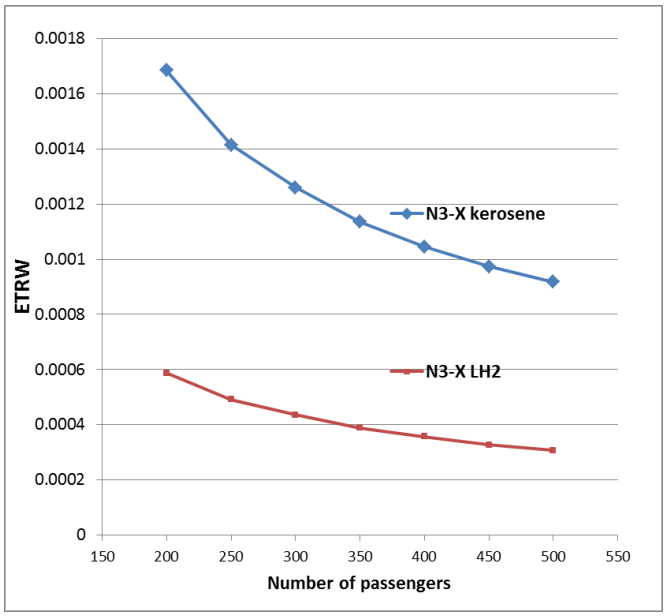

Figure 28: Payload fuel energy efficiency of the flight keeping range constant

In figure 30, the payload is kept constant while the target range was increased. In this case the N3-X-L has a constant benefit in terms of ETRW by a factor of 2 compared to the N3-X.

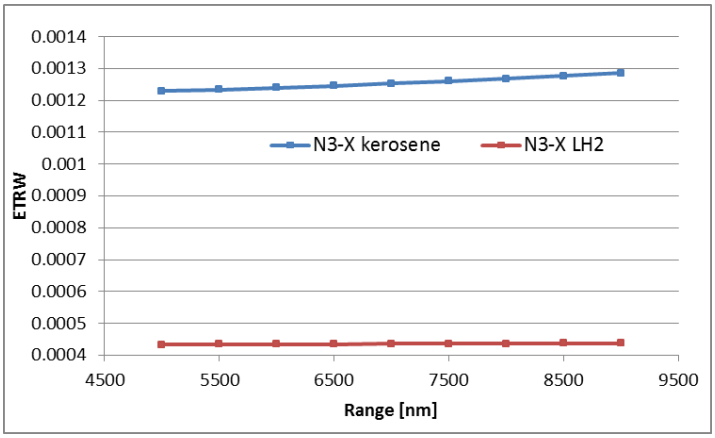

Figure 29: Payload fuel energy efficiency of the flight keeping the number of passengers constant

To assess the detrimental effects of the LH_2 tanks volume, the following procedure was followed. Initially, the required mission (in terms of range and passengers) was performed and the total volume available inside the forward centerbody section was calculated with FLOPS. By assuming a $30ft^3$ volume assigned to each passenger, the volume available for the fuel tanks was obtained. Then, without compromising the number of passengers, the reduced range was calculated based on the reduced fuel that could be stored. All the configurations were calculated for a constant OEW. The results can be seen in figure 31.

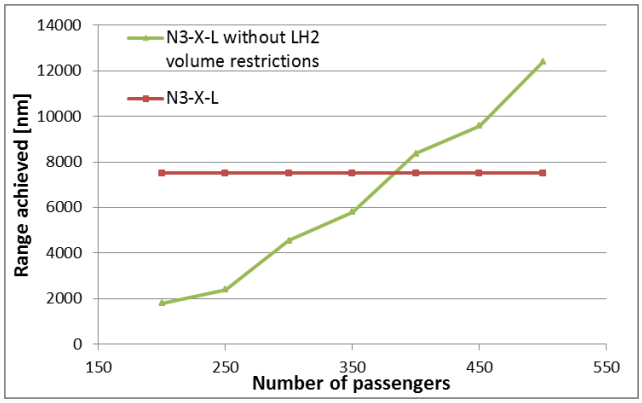

Figure 30: Range achieved for restricted and unrestricted N3-X-L configurations

4.3.3 N3-X using Thrust-Split

For this analysis, a TS ratio of 65% was selected and the power required can be seen in table 19.

TS ratio	Total Power Required [MW] at ADP	Total thrust required by core-engines [lbf (kN)] at ADP
95 %	21.2	971 (4.32)
65 %	13.2	7737 (34.42)

Table 19: Power required for different TS ratios

The TS ratio was defined at the design point and it was allowed to vary in off-design conditions. Another way to deal with TS in off-design cases would be to keep the TS ratio constant by varying the power requirements. For each TS ratio corresponds a power demand from the distributed propulsors and it was assumed that the power demand from the distributed propulsors remained constant in off-design conditions. For both Thrust-Split values, the BPR was

held constant while the FPR was varied to achieve minimum SFC. TET was used as a handle in order to match the thrust and power requirements. By using the distributed parameters in table 19, main engine turbofans of BPR 4, the fuel burn of the N3-X and N3-X-TS65 configurations was calculated as can be seen in figure 32.

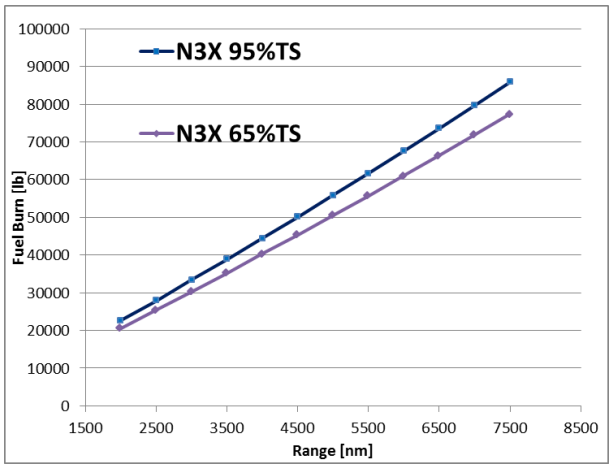

Figure 31: Fuel burn for different TS ratios

The configuration with the 65% TS ratio shows small fuel improvements that increase as the range increases. Since the weight of the propulsion system is higher for the 65% TS configuration, the fuel benefits are provided from the more fuel efficient propulsion system. Figure 33 shows a small improvement in the energy usage of the N3-X configuration using 65%TS. The benefits improved as the range increased. This may be attributed to the fact that as the range of the missions increase, the cruise segment dominates and hence the benefit from the advanced airframe (BWB and Boundary layer Ingestion) is more prevalent.

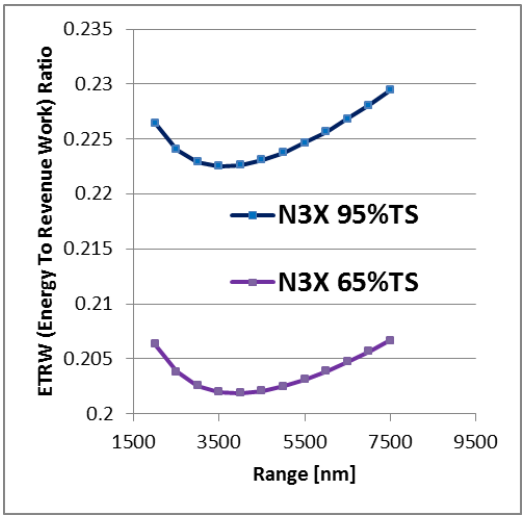

Figure 32: ETRW for different TS ratios

4.3.4 N3-x sensitivity analysis

This section presents the effect of the variation of design parameters in the mission energy consumption for the N3-X using 95% TS. In this thesis, 1% inlet pressure losses and 1% BLI penalty on the fan efficiency were assumed. Figures 34 and 35 show the sensitivity of these two parameters in the total mission energy consumption. The mission fuel mass was obtained from FLOPS and it was converted to mission energy consumption by multiplying with the LHV of kerosene.

The trends indicate that while both installation effects cause an increase in the energy consumption, efforts in reducing the inlet pressure losses have almost a double effect on the energy consumption than reducing the fan efficiency losses.

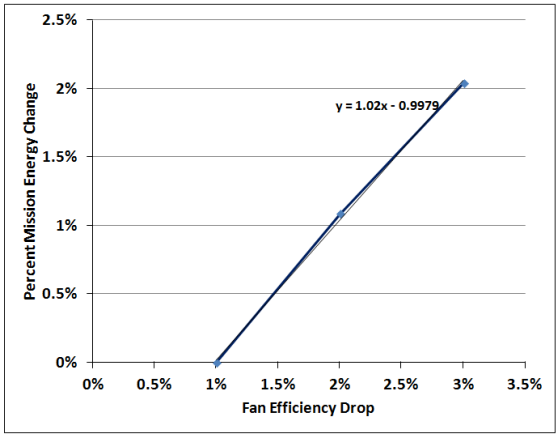

Figure 33: Effect of distributed Propulsor installations (fan efficiency) losses on Mission Energy consumption

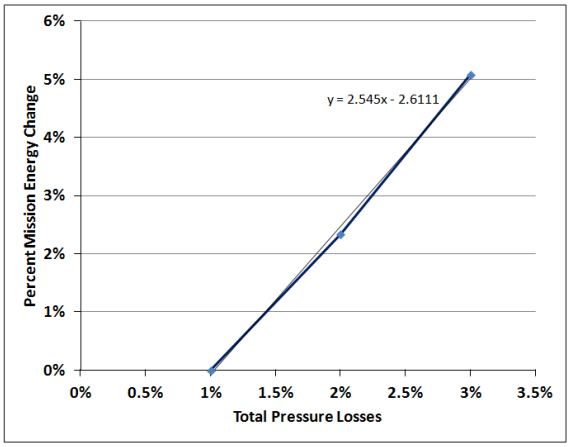

Figure 34: Effect of distributed Propulsor intake total pressure losses on Mission Energy consumption

For similar mission specifications, an investigation was also undertaken to analyse the sensitivity of the mission energy consumption to changes in the propulsion system weight whilst keeping the TSFC constant and vice versa. The propulsion weight referred to here, includes the weight of the core engines and the propulsor fans without the weight of the electrical and cooling system. Analyses of the trends clearly indicate the higher sensitivity of the mission energy consumption to an increase in TSFC than when compared to propulsion system weight and are similar to those reported in [17].

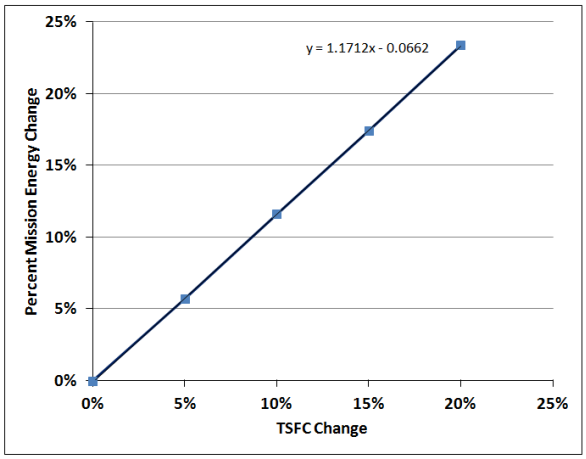

Figure 35: Effect of change in TSFC (assuming constant propulsion system weight) on Mission Energy consumption

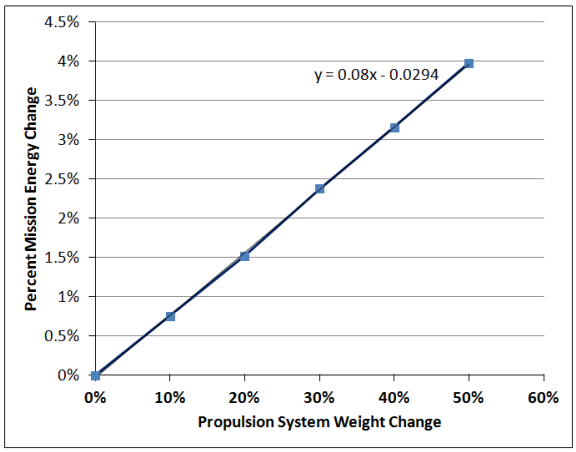

Figure 36: Effect of change in propulsion system weight (assuming constant TSFC) on Mission Energy consumption

5 Conclusions and future work

This thesis used a unique methodology was used to calculate the performance of a futuristic conceptual aircraft that employed Turboelectric Distributed Propulsion on a Blended-Wing-Body airframe with similar characteristics as the N3-X concept. Results showed that fuel benefits can be achieved through the higher effective BPR and by using Boundary-Layer-Ingestion. Additionally, the Thrust-Split ratio showed an increased performance but additional research must be performed because of the important amount of assumptions that were used.

Based on the assumptions of this thesis, the proposed future work should be focused in the following areas:

Airframe

- The drag due to the distributed propulsors array was not taken into account.
- The bending moment benefits due to the wing-tip core engines should be estimated.

Boundary-Layer Ingestion

- The Boundary Layer profiles used from NASA are only suitable for cruise conditions and a CFD research should be performed to find total pressure and Mach number inlet profiles at different angles of attack and conditions
- A very optimistic assumption of 1% was used for fan efficiency losses and pressure losses. An improved method of estimating the losses should be used

Distributed Propulsors

- The power was assumed constant at all conditions and the thrust produced from the distributed propulsors was calculated based on this assumption. It is advised that a power and thrust schedule during the

flight envelope is calculated in order to have an increased accuracy in the performance of the main engines and propulsor unit

Additional future work

To have a more holistic assessment of the TeDP some additional future work was identified by the author throughout this year and it is presented below.

- **Trade-off between aerodynamic and electrical efficiency of the TeDP system**

In the TeDP vehicle, the power is produced by the core engines and transmitted to the fans through superconducting motors and generators. Power inverters are used to decouple the generator and fan motor speeds. Furthermore, the power and speed in a given generator or motor are also independent of each other and this allows the generator to operate at a power level and shaft speed that yields the best performance.

In the literature, the fan always runs at its optimum speed and whether the motor runs at its optimum speed in the same time or not has not been covered at all. The speed of the fan is optimised based on the tip speed requirements but this speed is not optimum for the motor as a higher speed motor could be of smaller size. This is an important area of research according to the author's view. The research should focus on this trade-off and will have to establish an optimum rotational speed that will optimise the performance of both fan and motor simultaneously.

- **Rain Ingestion**

According to Dr.Nikolaidis [47] for a conventional T&W aircraft "the effects of water ingestion on gas turbine engines are aerodynamic (air shear force increase, change of velocity triangle in the compressor), thermodynamic (heat and mass transfer, temperature distortion, change of gas properties in the

working medium) and mechanical (demanded torque increase, blade vibration, change of structural load)".

For an aircraft using a TeDP system on a BWB airframe the effect will probably be enhanced for several reasons:

- Apart from the core-engines, there are numerous embedded distributed propulsors that will be influenced by rain ingestion
- Boundary Layer Ingestion is a very critical phenomenon and will be affected as the ingestion happens in all the upper airframe.
- The BWB airframe has a larger surface compared to a T&W aircraft and rain can accumulate easier.

The objective of the future work should be to investigate and quantify the performance deterioration of the propulsor fans of a TeDP vehicle due to water ingestion.

The proposed steps that should be followed are:

1. The identification of the factors that affect water flow in the propulsors of the TeDP vehicle under water ingestion conditions.
2. The evaluation of their impact on the propulsor performance
3. The evaluation of the total impact of rain ingestion in the performance of the TeDP system
4. Implement the effects of rain ingestion on the calculation of the power of the distributed propulsors.

- **Contrails**

The environmental requirements related to the latest timeframe, N+3, include reducing Landing and Take-off (LTO) NOx by 60%, compared to current generation aircraft, reducing cruise NOx and CO2, and a way to diminish the formation of contrails.

The conceptual aircraft N3-X will alter the amount of emissions produced and also if Liquid Hydrogen (LH2) is to be used as a fuel then contrail emissions will

be significantly higher. The aim of this assessment should be to evaluate the potential of this novel configuration to reduce the formation of persistent contrails.

REFERENCES

[1] "D. Dagget, "Alternative Fuelled Aircraft," Boeing, Presentation 2006.", .

[2] *, GE-90 Technical specification engine database, available at: http://www.geaviation.com/commercial/engines/ge90, sourced on 26 July 2014*.

[3] "Dr K W Ramsden, Turbomachinery Course notes - Compressors, Cranfield: Cranfield University,", (2013), in .

[4] Agarwal, R. K. and Zhang, Z. (2011), *Optimization of ETRW (Energy Liberated During a Flight/Revenue Work Done) of an Airplane for Minimizing its Environmental Impact,* .

[5] Airbus *, Global Market Forecast 2013-2032*, available at: http://www.airbus.com/company/market/forecast/ (accessed 12/12).

[6] Ameyugo, G., Taylor, M. and Singh, R. (2006), "Distributed propulsion feasibility studies", *25th International Congress of the Aeronautical Sciences,* pp. 06.

[7] Ameyugo, G., Taylor, M. and Singh, R. (2006), "Distributed propulsion feasibility studies", *25th International Congress of the Aeronautical Sciences,* pp. 06.

[8] Basam, V. R. and Das, A. (2010), "All Electric Ship-The Super Platform for Tomorrow's Naval Warfare", *Proceeding of Naval Armaments, CII, New Delhi,* .

[9] Boeing *, B777-200LR technical characteristics*, available at: http://www.boeing.com/boeing/commercial/airports/777.page (accessed 2014).

[10] Brewer, G. D. (1991), *Hydrogen aircraft technology,* CRC.

[11] Brown, G. V. (2011), "Weights and efficiencies of electric components of a turboelectric aircraft propulsion system", *49th AIAA Aerospace Science Meeting, Orlando, Fl,* .

[12] Bushnell, D. M. (1997), "Frontiers of the" Responsibly Imaginable" in (civilian) Aeronautics", .

[13] Colozza, A. J. (2002), *Hydrogen storage for aircraft applications overview,* National Aeronautics and Space Administration, Glenn Research Center.

[14] Daly, M. and Gunston, B. (2007), "Jane's Aero-Engines", *Jane's Information Group,* .

[15] Drela, M. (2009), "Power balance in aerodynamic flows", *AIAA Journal,* vol. 47, no. 7, pp. 1761-1771.

[16] Feagin, R. C. and Morrison, W. D. (1978), *Delta Method, Empirical Drag Build-up Technique: Final Report,* Lockheed-California Company.

[17] Felder, J. L., Brown, G. V., DaeKim, H. and Chu, J. (2011), "Turboelectric Distributed Propulsion in a Hybrid Wing Body Aircraft", .

[18] Felder, J. L., Kim, H. D. and Brown, G. (2009), "Turboelectric distributed propulsion engine cycle analysis for hybrid-wing-body aircraft", *AIAA Paper,* vol. 1132, pp. 2009.

[19] Felder, J. L., Kim, H. D. and Brown, G. V. (2009), "Turboelectric distributed propulsion engine cycle analysis for hybrid-wing-body aircraft", *AIAA Paper,* vol. 1132, pp. 2009.

[20] Felder, J. L., Kim, H. D., Brown, G. V. and Chu, J. (2011), "An examination of the effect of boundary layer ingestion on turboelectric distributed propulsion systems", *AIAA Paper,* vol. 300, pp. 2011.

[21] Felder, J. L., Tong, M. T. and Chu, J. (2012), "Sensitivity of Mission Energy Consumption to Turboelectric Distributed Propulsion Design Assumptions on the N3-X Hybrid Wing Body Aircraft", *48th AIAA/ASME/SAE/ASEE Joint Propulsion Conference & Exhibit,* .

[22] Gerend, R. P. and Roundhill, J. P. (1970), "Correlation of gas turbine engine weights and dimensions", *AIAA paper,* vol. 669, pp. 1970.

[23] Gohardani, A. S., Doulgeris, G. and Singh, R. (2011), "Challenges of future aircraft propulsion: a review of distributed propulsion technology and its potential application for the all electric commercial aircraft", *Progress in Aerospace Sciences,* vol. 47, no. 5, pp. 369-391.

[24] Gohardani, A. S., Doulgeris, G. and Singh, R. (2011), "Challenges of future aircraft propulsion: A review of distributed propulsion technology and its potential application for the all electric commercial aircraft", *Progress in Aerospace Sciences,* vol. 47, no. 5, pp. 369-391.

[25] Greitzer, E. M., Bonnefoy, P., DelaRosaBlanco, E., Dorbian, C., Drela, M., Hall, D., Hansman, R., Hileman, J., Liebeck, R. and Lovegren, J. (2010), "N 3 Aircraft Concept Designs and Trade Studies", .

[26] Haglind, F., Hasselrot, A. and Singh, R. (2006), "Potential of reducing the environmental impact of aviation by using hydrogen. Part I: background,

prospects and challenges", *Aeronautical Journal,* vol. 110, no. 1110, pp. 533-540.

[27] Hileman, J., Spakovszky, Z., Drela, M. and Sargeant, M. (2007), "Airframe design for silent aircraft", *AIAA paper,* vol. 453, pp. 2007.

[28] Hill, G. A. and Thomas, R. H. (2004), "Challenges and Opportunities for Noise reduction through advanced aircraft propulsion airframe integration and configurations", *8th CEAS Workshop on Aeroacoustics of New Aircraft and Engine Configurations, Budapest, Hungary,* .

[29] J Clavier (2007), *Aero gas turbine engine design project (AVIC) ultra high by-pass ratio (12-14) study* (PhD thesis), Cranfield, .

[30] Jane, F. T. (1909), *Jane's all the world's aircraft,* McGraw-Hill.

[31] Kim, H. D., Berton, J. J. and Jones, S. M. (2006), "Low noise cruise efficient short take-off and landing transport vehicle study", *AIAA Paper,* vol. 7738, pp. 2006.

[32] Kim, H. D. (2010), "Distributed propulsion vehicles", *27th International Congress of the Aeronautical Sciences,* .

[33] Kim, H. D., Brown, G. V. and Felder, J. L. (2008), "Distributed turboelectric propulsion for hybrid wing body aircraft", *9th International Powered Lift Conference, London, United Kingdom,* .

[34] Kim, H. D., Brown, G. V. and Felder, J. L. (2008), "Distributed turboelectric propulsion for hybrid wing body aircraft", *9th International Powered Lift Conference, London, United Kingdom,* .

[35] Kim, H. D. and Felder, J. L. (2011), "Control volume analysis of Boundary Layer Ingesting propulsion systems with or without shock wave ahead of the inlet", *49th AIAA Aerospace Sciences Meeting, American Institute of Aeronautics and Astronautics, Reston, VA (submitted for publication),* .

[36] Kim, H. and Liou, M. (2013), "Shape design optimization of embedded engine inlets for N2B hybrid wing-body configuration", *Aerospace Science and Technology,* vol. 30, no. 1, pp. 128-149.

[37] Kirner, R. (2013), "An investigation into the benefits of distributed propulsion on advanced aircraft configurations", .

[38] Küchemann, D. and Weber, J. (1953), *Aerodynamics of propulsion,* McGraw-Hill.

[39] Lapedra Alexandre (2014), *Blended Wing Body and Distributed Propulsion LH_2 application as Fuel* (MSc thesis), Cranfield University, Cranfield University.

[40] Liebeck, R., Page, M. and Rawdon, B. (1998), "Blended-wing-body subsonic commercial transport", *AIAA paper,* vol. 438.

[41] Liu, C. (2014), *Turboelectric Distributed Propulsion System Modelling* (PhD thesis), CRANFIELD UNIVERSITY, .

[42] Liu, C., Doulgeris, G., Laskaridis, P. and Singh, R. (2013), "Thermal cycle analysis of turboelectric distributed propulsion system with boundary layer ingestion", *Aerospace Science and Technology,* vol. 27, no. 1, pp. 163-170.

[43] Liu, C., Ihiabe, D., Laskaridis, P. and Singh, R. (2013), "A preliminary method to estimate impacts of inlet flow distortion on boundary layer ingesting propulsion system design point performance", *Proceedings of the Institution of Mechanical Engineers, Part G: Journal of Aerospace Engineering,* , pp. 0954410013496750.

[44] Mankins, J. C. (1995), "Technology readiness levels", .

[45] Manneville, A., Pilczer, D. and Spakovszky, Z. (2004), "Noise reduction assessments and preliminary design implications for a functionally-silent aircraft", *AIAA paper,* vol. 2925, pp. 2004.

[46] McCullers, A. (2003), "FLOPS User's Guide–Release 6.02", *NASA Langley Research Center,* .

[47] Nikolaidis, T. (2008), *Water ingestion effects on gas turbine engine performance* (PhD thesis), Cranfield, .

[48] Osborn, W. M., Moore, R. D. and Steinke, R. J. (1978), "Aerodynamic performance of a 1. 35-pressure-ratio axial-flow fan stage", .

[49] Patterson, J. C. and Flechner, S. G. (1970), *An exploratory wind-tunnel investigation of the wake effect of a panel tip-mounted fan-jet engine on the lift-induced vortex,* National Aeronautics and Space Administration, Scientific and Technical Information Branch.

[50] Pera, R.J., Onat, E., Klees, G.W., Tjonneland, E (1977), *A method to estimate weight and dimensions of aircraft gas turbine engines. Volume 1: Method of analysis,* NASA CR-135170.

[51] Plas, A., Sargeant, M., Madani, V., Crichton, D., Greitzer, E., Hynes, T. and Hall, C. (2007), "Performance of a boundary layer ingesting (BLI) propulsion system", *Paper No.AIAA-2007-0450,* .

[52] Rodriguez, D. L. (2001), *A multidisciplinary optimization method for designing boundary layer ingesting inlets,* .

[53] Sagerser, D. A., Lieblein, S. and Krebs, R. P. (1971), *Empirical expressions for estimating length and weight of axial-flow components of VTOL powerplants,* National Aeronautics and Space Administration.

[54] Savino Depalo (2013), *Modelling of Distributed Propulsion system with Boundary Layer Ingestion* (MSc thesis), Cranfield University, Cranfield University.

[55] Sehra, A. K. and Whitlow, W. (2004), "Propulsion and power for 21st century aviation", *Progress in Aerospace Sciences,* vol. 40, no. 4, pp. 199-235.

[56] Sekaran, P. R., Gohardani, A. S., Doulgeris, G. and Singh, R. (2013), "Liquid hydrogen tank considerations for turboelectric distributed propulsion", *Aircraft Engineering and Aerospace Technology,* vol. 86, no. 1, pp. 67-75.

[57] Smith, A. (2012), "The jet airplane utilizing boundary layer air for propulsion", *Journal of the Aeronautical Sciences (Institute of the Aeronautical Sciences),* vol. 14, no. 2.

[58] The Boeing Company *, Current Market Outlook 2013-2032*, available at: http://www.boeing.com/boeing/commercial/cmo/index.page? (accessed 12/12).

[59] Valencia, E. A., Nalianda, D., Laskaridis, P. and Singh, R. (2014), "Methodology to assess the performance of an aircraft concept with distributed propulsion and boundary layer ingestion using a parametric approach", *Proceedings of the Institution of Mechanical Engineers, Part G: Journal of Aerospace Engineering,* , pp. 0954410014539291.

[60] Verstraete, D. (2009), "The potential of liquid hydrogen for long range aircraft propulsion", .

APPENDICES

Appendix A Core weight estimation

This section contains the steps used to calculate the weight of the core-engines. It was adapted from [54]. The components (and their sub-parts) that compose the total weight of the core-engines are listed in table 20 together with the main assumptions used. The next sections describe in details the way that each component weight was calculated.

• Components	• Parts	• Assumptions
• Fan	• Rotor blades • Rotor hub and spinner • Stator blades • Outer casing • Support struts	• Inlet Mach number = 0.6 • AR = 2.5-3.5 • Dh/Dt = 0.3-0.4 • • For Distributed Propulsor fans and duct: • Duct casing thickness is 1.3mm • Wall thickness is 1mm • Aluminium density : 2770 kg/m
• Compressor (LPC, HPC)	• Rotor blades • Disks (or drum) • Seals • Stator blades • Casing	•
• Combustor	• Inner and outer casing • Liner • Fuel nozzle	• An annular axial flow combustor is considered because of the lower pressure losses than the other combustor type •

		• Inlet combustor velocity: 18.3m/s [53]
• Turbine (HPT, LPT)	• Rotor disk and blades • Stator blades • Seals • Casing	• HPT number of stages = 2 • LPT number of stages = 6 •

Table 20: Parts and assumptions for each component weight estimation

Fan weight calculations

Initially the inlet fan area, A1, is calculated. This requires the total conditions that are obtained from TURBOMATCH simulations and the inlet Mach number is assumed to be 0.7.

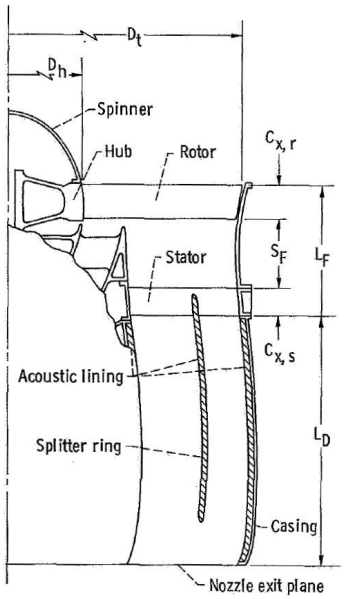

Figure 37: Fan stage and duct model [53]

The inlet area is calculated with equation:

$$A_1 = \frac{W_{tot}}{\rho_1 C_1} \quad \text{(D.1)}$$

Where density ρ and velocity C are calculated with equations:

$$t_1 = \frac{T_1}{1+\frac{\gamma-1}{2}M_1^2} \quad \text{(D.2)}$$

$$p_1 = P_1\left(\frac{t_1}{T_1}\right)^{\frac{\gamma}{\gamma-1}} \quad \text{(D.3)}$$

$$\rho_1 = \frac{p_1}{Rt_1} \quad \text{(D.4)}$$

$$C_1 = M_1\sqrt{\gamma R t_1} \quad \text{(D.5)}$$

Then according to Sagerser [53] the fan weight is calculated by:

$$W_F = K_{fan} D_{t,1}^{2,7} \frac{N}{AR^{0.5}} \left[\frac{\sigma_t}{(\sigma_t)_{ref}}\right]^{0.3} \left[\frac{U_t}{(U_t)_{ref}}\right]^{0.3} \quad \text{(D.6)}$$

Where $(\sigma_t)_{ref}$ = 1.25 , $(U_t)_{ref}$ =350 m/s and K_{fan} = 135 (for cruise engines). The value of $D_{t,1}$ comes from the following equations:

$$A_1 = \frac{\pi(D_t^2 - D_h^2)}{4} \quad \text{(D.7)}$$

$$\frac{D_h}{D_t} = 0.4 \quad \text{(D.8)}$$

Compressor weight calculations

The Inlet and outlet area were found in the same way as was shown for the fan considering different Inlet and outlet Mach numbers and also hub/tip ratios for LPC and HPC that were taken from Ramsden [3].

Then according to Sagerser [53] the weight is calculated by:

$$W_{comp} = K_{comp} D_M^{2,2} N^{1.2} \left[1 + \frac{\frac{L_C}{D_{M,1}}}{\left(\frac{L_C}{D_{M,1}}\right)_{ref}}\right] \left[\frac{U_t}{(U_t)_{ref}}\right]^{0.5} \quad \text{(D.9)}$$

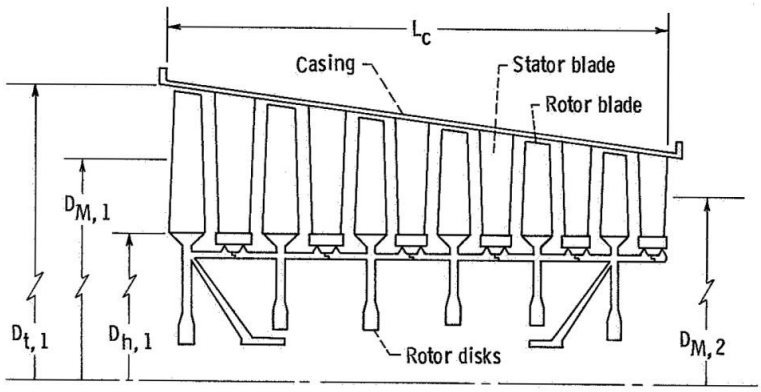

Figure 38: Compressor model [53]

Where:

- K_{comp} = 24.2 (for cruise engines)
- DM is the average between the mean diameter at inlet and outlet calculated with equation (D.10). The values of hub and tip diameter come from equations (D.7) and (D.8) while keeping in mind that the hub to tip diameter ratio is different from the fan.

$$D_M = \frac{1}{2}(D_{M,1} + D_{M,2}) \quad \text{(D.10)}$$

$$D_{M,1/2} = \frac{1}{2}(D_{t,1-2} + D_{h,1-2}) \quad \text{(D.11)}$$

- The number of stages has been calculated by equation (D.12) where PR_{stage} is equal to 1.4 and PR is equal to the pressure ratio for low or high pressure compressor depending on the case.

$$N = \text{int}\left(\frac{PR}{PR_{stage}}\right) \quad \text{(D.12)}$$

- The ratio between the compressor length and the mean inlet diameter is obtained from equation (D.13)

$$\frac{L_C}{D_{M,1}} = 0.2 + [0.234 - 0.218\left(\frac{D_h}{D_t}\right)_1] N \quad \text{(D.13)}$$

- The reference length upon the mean inlet diameter can be calculated by using equation (D.13) for a value of inlet hub to tip diameter ratio equal to 0.7.

- The reference value for U_t is 335 m/s.
- For the LPC the value of U_t results from the equation (D.8) because of the fan and this compressor are fixed on the same shaft and hence they have the same rotational speed. For the HPC U_t is chosen equal to $(U_t)_{ref}$.

$$(U_t)_{LPC} = \frac{(D_{t,1})_{LPC}}{(D_{t,1})_{fan}}(U_t)_{fan} \qquad \text{(D.14)}$$

Combustor weight calculations

The average between the mean diameter at inlet and outlet is calculated with the same procedure considering an inlet and outlet Mac number of 0.3 and an inlet/outlet hub to tip diameter ratio of 0.85/0.8.

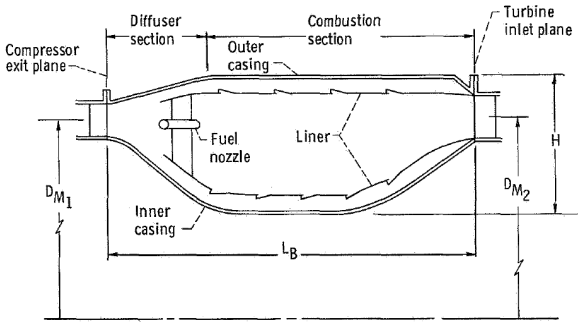

Figure 39: Combustor model

Equation (D.15) is used to determine the combustor weight.

$$W_{burner} = K_{burner} D_M^2 \left[\frac{\frac{L_B}{H}}{\left(\frac{L_B}{H}\right)_{ref}} \right]^{0.5} \qquad \text{(D.15)}$$

Where:

- Kburner = 390 (for cruise engines)
- LB/H is chosen equal to (LB/H)ref which is equal to 3.2 for cruise engines

To calculate H and therefore LB, equation (D.16) is used. The flow velocity, Vref, in the combustion chamber for a cruise engine is assumed 18.3 m/s.

$$H = \frac{W_1}{\rho_1 \pi D_M V_{ref}} \qquad \text{(D.16)}$$

Turbine weight calculations

The average between the mean diameter at inlet and outlet is calculated with the same procedure as above by considering for HPT, LPT and FPT an inlet/outlet Mac number respectively of 0.3/0.4, 0.4/0.5, 0.5/0.5 and an inlet/outlet hub to tip diameter ratio of 0.9/0.7 for all the turbines.

Equation (D.17) is used to determine the turbine weight.

$$W_{turb} = K_{turb} D_M^{2.5} N U_M^{0.6} \qquad \text{(D.17)}$$

where Kturb is 7.9 (for cruise engines) and the number of stages N for each turbine is listed in table 20. The values for the average mean blade velocity are found with equation (D.18) for HPT (same shaft of HPC) and equation (D.19) for LPT (same shaft of fan and LPC).

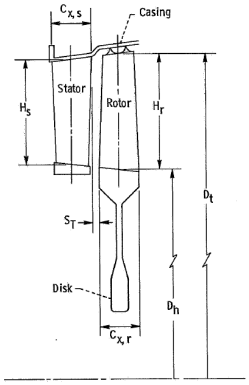

Figure 40: Turbine stage diagram

$$(U_M)_{HPT} = \frac{(D_M)_{HPT}}{(D_{t,1})_{HPC}} (U_t)_{HPC} \qquad \text{(D.18)}$$

$$(U_M)_{LPT} = \frac{(D_M)_{LPT}}{(D_{t,1})_{LPC}} (U_t)_{LPC} = \frac{(D_M)_{LPT}}{(D_{t,1})_{fan}} (U_t)_{fan} \qquad \text{(D.19)}$$

Appendix B LH2 tank weight estimation

The total LH2 tank weight consists of the tank mass, boil-off mass and the insulation.

B.1 **Calculation of the boil-off mass**

To calculate the boil off mass we need to make an estimation of the heat transfer in the tank. To do that, we have three different sources of heat transfer, conduction, convection and radiation:

$$Q_{convection} = h \times (T_\infty - T_s) \quad \textbf{(A-1)}$$

$$Q_{radiation} = \epsilon\sigma \times (T_\infty^4 - T_s^4) \quad \textbf{(A-2)}$$

$$Q_{conduction} = \frac{T_s - T_{LH2}}{R_{th}} \quad \textbf{(A-3)}$$

Where:

- T_S: the temperature of the tank
- T_∞: the exterior temperature
- ε: the emissivity
- R_{th}: , the thermal resistance of the tank
- σ: Stefan-Boltzmann constant

The surface of the tank can be divided into two shapes, a cylinder and a sphere:

$$R_{th,sphere} = \frac{1}{4.\pi.\lambda} \times \left(\frac{1}{R_1} - \frac{1}{R_2}\right) \quad \textbf{(A-4)}$$

$$R_{th,cylinder} = \frac{\ln\left(\frac{R_2}{R_1}\right)}{2.\pi.\lambda.L} \quad \textbf{(A-5)}$$

The last thing to calculate is the convection heat transfer. We will use the expression of non-dimensional number found in [13].

$$Nu = \frac{h.D}{K_g} \quad \textbf{(A-6)}$$

$$\mathrm{Pr} = \frac{\nu}{\alpha} \quad \textbf{(A-7)}$$

$$R_{ad} = \frac{g.\beta.(T_\infty - T_s).D^3}{\nu.\alpha} \quad \textbf{(A-8)}$$

Where:

- Nu: Nusselt number
- Pr: Prandtl number
- R_{ad}: Rayleigh number
- v: Viscosity of the air
- α: Gas diffusivity

$$\alpha = -3.119\times10^{-6} + 3.541\times10^{-8}.T_\infty + 1.679\times10^{-10}.T_\infty^2 \quad \textbf{(A-9)}$$

$$\nu = -2.079\times10^{-6} + 2.777\times10^{-8}.T_\infty + 1.077\times10^{-10}.T_\infty^2 \quad \textbf{(A-10)}$$

The expression for the Nusselt number for a sphere and a cylinder respectively is given by:

$$N_{UD} = 2 + \frac{0.589.R_{ad}^{\frac{1}{4}}}{\left[1 + \left(\frac{0.469}{\Pr}\right)^{\frac{9}{16}}\right]^{\frac{4}{9}}} \quad \textbf{(A-1)}$$

$$N_{UD} = \left\{0.6 + \frac{0.387.R_{ad}^{\frac{1}{6}}}{\left[1 + \left(\frac{0.559}{\Pr}\right)^{\frac{9}{16}}\right]^{\frac{8}{27}}}\right\}^{2} \quad \textbf{(A-12)}$$

The only unknown in all those equations is the temperature of the tank wall. To find the right temperature we have to verify the conservation of energy, that is to say that the convection plus the radiation is equal to the conduction:

$$Q_{cond} = Q_{conv} + Q_{rad} \quad \textbf{(A-13)}$$

So the next step will be guess this temperature and through an iterative process to calculate all the heat transfer. When the temperature is known then all the heat transfers are calculated. This will enable us to obtain the mass of boil off in the tank:

$$M = \frac{Q_{conv} + Q_{rad}}{h_{fg}} \quad \textbf{(A-4)}$$

Where:

- M: Boil off rate
- H_{fg}: Heat of vaporization of liquid hydrogen (446592 J/kg)

B.2 **Choice of insulation material**

For the design of the tank, the insulation material is required. Since we look into an aircraft application, we want a light material with the minimum mass per unit of volume. Additionally, the thermal conductivity must be kept as low as possible. Some of the potential materials that can be used for aircraft application can be seen in figure 42 [60] and Table 21 [13].

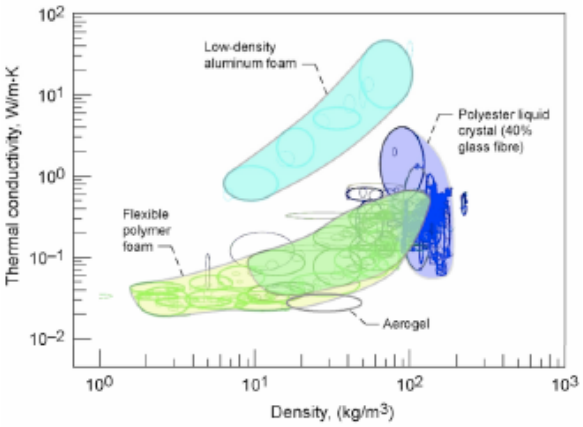

Figure 41: Thermal conductivity against density [60]

Insulation type	Density (kg/m^3)	Thermal conductivity (W/mK)
Rigid closed cell polymethacrylimide	35.3	0.0096

Rigid open cell polyurethane	32.1	0.0112
Rigid closed cell polyvinalchloride	49.8	0.0046
Rigid closed cell polyurethane and chopped glass fiber	64.2	0.0064
Evacuated aluminium foil separated with fluffy glass mats	40	0.00016
Evacuated aluminium foil and glass paper laminate	120	0.000017
Evacuated silica powder	160	0.00017

Table 21: List of insulation materials [13]

As the goal is to minimize the density and the thermal conductivity, the product of these two parameters has been compared in figure 43.

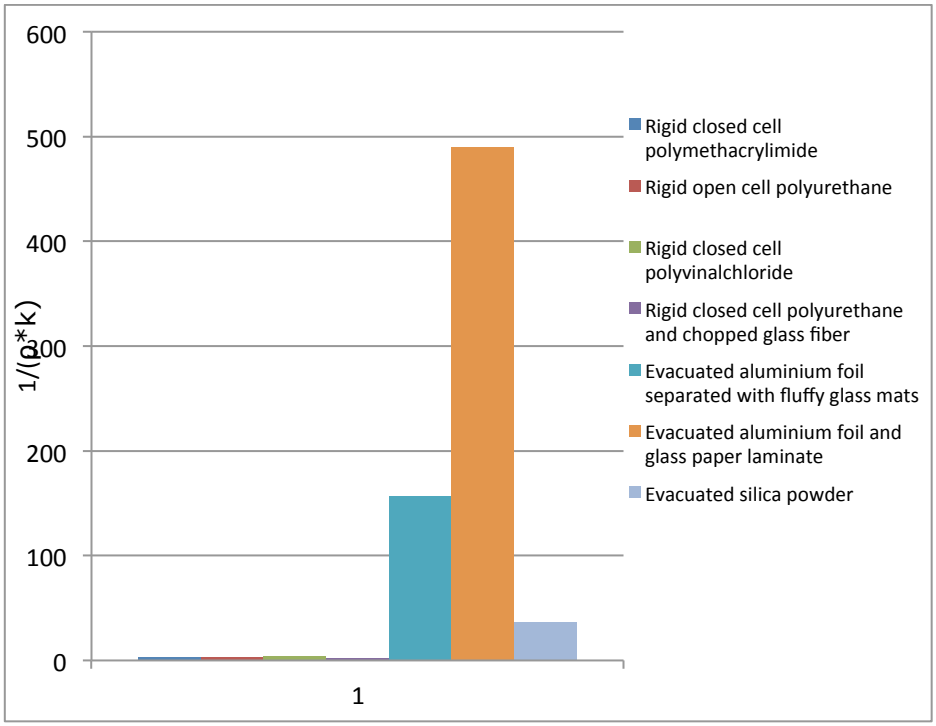

Figure 42; Insulation materials properties

The results show that the evacuated aluminium foils are probably the two best materials to insulate the tank. To find the most appropriate, the boil off weight was calculated for these two materials for different radius of tank at constant length. The boil off time the mass of the tank, plotted against the radius of the tank, can be seen below:

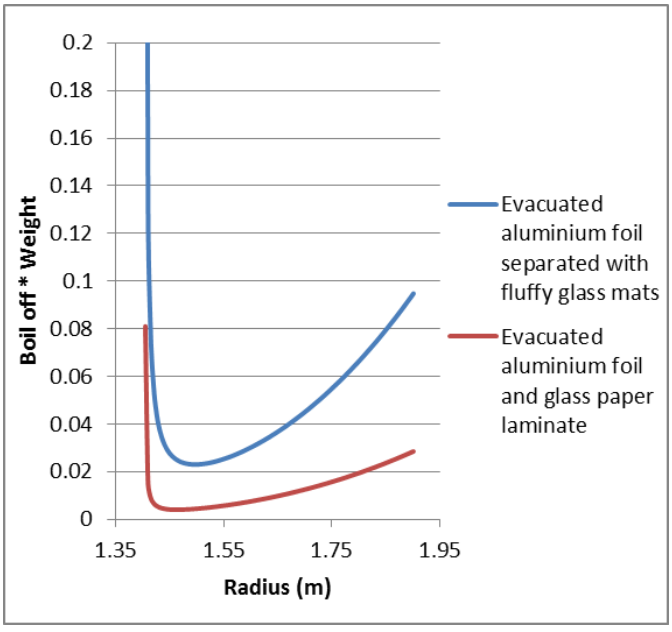

Figure 43: Tank insulation materials results

It can be observed that the “evacuated aluminium foil and glass paper laminate” is the material offering the best compromise between boil off and the weight of the tank. This material will be considered in this thesis.

Appendix C N3-X geometry

The data extracted from the N3-X configuration in OpenVSP is summarized in table 22. The different sections that correspond to different stations in the wings can be seen in figure 45. For display purposes section 11 is highlighted in red.

	Section 1	Section 2	Section 3	Section 4	Section 5	Section 6	Section 7
Airfoil	N2A root	N2A 072	N2A 072	N2A 072	N2A 125	N2A 192	N2A 269
Thickness / chord	0.132	0.132	0.132	0.133	0.134	0.125	0.0975
Span [ft]	1.54	1.72	2.92	3.78	8.43	4.99	10.33
Span [m]	0.462	0.516	0.876	1.134	2.529	1.497	3.099
Tip Chord [ft]	133.81	132.6	127.2	116.58	86.27	71.12	46.49
Tip Chord [m]	40.143	39.78	38.16	34.974	25.881	21.336	13.947
Root Chord [ft]	134.5	132.4231	126.9579	116.3	87	72.2	46.9
Root Chord [m]	40.29	40.11	39.72	38.16	34.974	25.881	21.336
Taper ratio	0.995	1.001	1.002	1.002	0.992	0.985	0.991
Sweep	29.2496	32.6025	55.1972	62.1632	66.8936	53.7263	42.7519
Sweep loc	0.25	0.25	0.25	0.25	0.25	0.25	0.25
Dihedral	-13	0	0	-10	0	-17	3

	Section 8	Section 9	Section 10	Section 11	Section 12	Section 13
Airfoil	N2A 354	N2A 354	N2A 445	N2A 585	N2A 800	N2A tip
Thickness / chord	0.07	0.065	0.05	0.01	0.01	0.01
Span [ft]	6.02	6.37	17.38	17.9	17.56	8.5
Span [m]	1.806	1.911	5.214	5.37	5.268	2.55
Tip Chord [ft]	35.47	28.58	20.83	15.67	10.33	8.2
Tip Chord [m]	10.641	8.574	6.249	4.701	3.099	2.46
Root Chord [ft]	36.1	29.2	21.1	15.6	10.3	8.2
Root Chord [m]	13.947	10.641	8.574	6.249	4.701	3.099
Taper ratio	0.983	0.979	0.987	1.004	1.003	1
Sweep	37.2334	20.7604	25.374	25.0355	24.8534	25.4786
Sweep loc	0.25	0.25	0.25	0.25	0.25	0.25
Dihedral	20.7462	-10	1.6667	-2	-4	10

Table 22: N3-X geometrical data

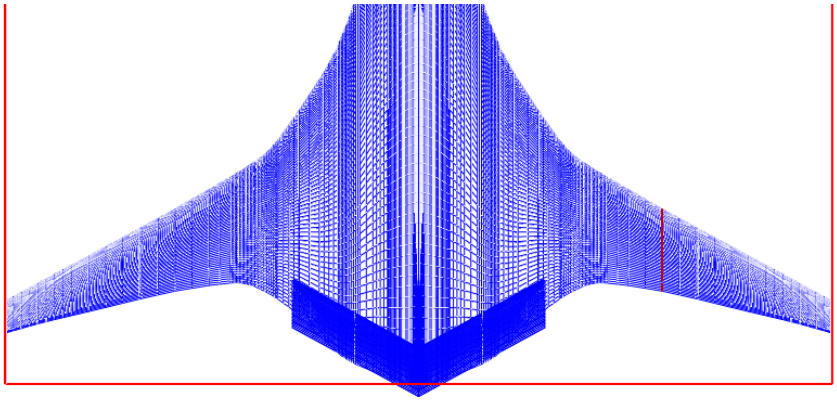

Figure 44: Top view of the N3-X configuration in OpenVSP